Journal of Medicinal Chemistry

Article

Structure-Based Design of Macrocyclic Factor XIa Inhibitors: Discovery of the Macrocyclic Amide Linker.

James R. Corte, Tianan Fang, Honey Osuna, Donald J. P. Pinto, Karen A Rossi, Joseph E Myers, Steven Sheriff, Zhen Lou, Joanna J Zheng, Timothy W. Harper, Jeffrey M. Bozarth, Yiming Wu, Joseph M Luettgen, Dietmar A Seiffert, Carl P. Decicco, Ruth R. Wexler, and Mimi L Quan

J. Med. Chem., **Just Accepted Manuscript** • DOI: 10.1021/acs.jmedchem.6b01460 • Publication Date (Web): 13 Jan 2017

Just Accepted

ACS Publications

Journal of Medicinal Chemistry is published by the American Chemical Society. 1155 Sixteenth Street N.W., Washington, DC 20036

Structure-Based Design of Macrocyclic Factor XIa Inhibitors: Discovery of the Macrocyclic Amide Linker.

James R. Corte[*], *Tianan Fang, Honey Osuna, Donald J. P. Pinto, Karen A. Rossi, Joseph E. Myers Jr., Steven Sheriff, Zhen Lou, Joanna J. Zheng, Timothy W. Harper, Jeffrey M. Bozarth, Yiming Wu, Joseph M. Luettgen, Dietmar A. Seiffert, Carl P. Decicco, Ruth R. Wexler and Mimi L. Quan*

Bristol-Myers Squibb Company, Research and Development, P.O. Box 5400, Princeton, New Jersey 08543, United States

KEYWORDS. Factor XIa; FXIa; Factor XIa Inhibitors; FXIa Inhibitors; Thrombosis; Activated Partial Thromboplastin Time; aPTT; Macrocycle; Anticoagulant; Antithrombotic.

ABSTRACT. A novel series of macrocyclic FXIa inhibitors was designed based on our lead acyclic phenyl imidazole chemotype. Our initial macrocycles, which were double-digit nanomolar FXIa inhibitors, were further optimized with assistance from utilization of structure-based drug design and ligand bound X-ray crystal structures. This effort resulted in the discovery of a macrocyclic amide linker which was found to form a key hydrogen bond with the carbonyl of Leu41 in the FXIa active site resulting in potent FXIa inhibitors. The macrocyclic

[*] Corresponding author. Tel.: +1-609-466-5030; fax: +1-609-818-3331; e-mail: james.corte@bms.com

FXIa series, exemplified by compound **16**, had a FXIa Ki = 0.16 nM with potent anticoagulant activity in an in vitro clotting assay (aPTT $EC_{1.5x}$ = 0.27 μM) and excellent selectivity against the relevant blood coagulation enzymes.

INTRODUCTION

Cardiovascular diseases remain the leading cause of death worldwide, accounting for 17.3 million deaths in 2013.[1] Two thirds of these deaths were attributed to ischemic heart disease and ischemic stroke which arises when an occlusive clot or thrombus forms in the circulation.[1] Antithrombotic therapies, such as anticoagulant or antiplatelet agents, have been developed to prevent the formation of thrombi but they are also accompanied by an increase in the risk of bleeding. Achieving an optimal balance between preventing an ischemic event and minimizing the risk of bleeding is central to a successful antithrombotic therapy. Recently approved novel oral anticoagulants (NOACs), such as direct Factor Xa inhibitors (rivaroxaban, apixaban, and edoxaban) and direct thrombin inhibitor (dabigatran), are highly effective for the prevention and treatment of cardiovascular events such as deep vein thrombosis (DVT), pulmonary embolism, and stroke from non-valvular atrial fibrillation.[2] These NOACs exhibited a favorable benefit-risk profile in the indications mentioned above, and in fact, displayed a significant reduction in intracranial bleeding when compared to warfarin in the stroke prevention studies.[2] However, NOACs have not shown a favorable benefit-risk profile in preventing venous thromboembolism (VTE) in medically ill patients[3] or in secondary prevention of acute coronary syndrome[4] (ACS) where an increased risk of bleeding has been observed.[5] Anticoagulants that are efficacious and show a reduced bleeding risk have the potential to address the unmet medical needs of patients.

Trypsin-like serine protease Factor XIa (FXIa), the activated form of the zymogen Factor XI (FXI), is an important enzyme in the intrinsic pathway of the blood coagulation cascade.[6]

FXIa plays a critical role in the amplification of thrombin generation which leads to the growth and maturation of thrombi.[6] Humans with a genetic deficiency in FXI (Hemophilia C) display a minor bleeding tendency which is in stark contrast to the abnormal, spontaneous and often times severe bleeding that is seen in humans with a genetic deficiency in either Factor VIII (Hemophilia A) or Factor IX (Hemophilia B).[7] Epidemiological studies suggest that a FXI deficiency may offer protection against pathologic thrombosis. Individuals with a severe FXI deficiency have a lower risk for ischemic stroke and DVT.[8] In addition, individuals with elevated levels of FXI are at a higher risk of acute myocardial infarction and DVT.[9] Since FXIa appears to contribute to thrombosis risk, but has a limited role in hemostasis, inhibition of either FXI or FXIa could provide an effective anticoagulant therapy with a safer bleeding profile.[10]

Both neutralizing antibodies[11] and antisense oligonucleotides[12] (ASO) which specifically target FXI have been shown be effective in a number of animal thrombosis models with minimal effects on bleeding time. In a Phase II clinical trial in total knee arthroplasty, an antisense oligonucleotide IONIS-FXIRx (formerly ISIS-FXIRx) was superior to enoxaparin for the prevention of DVT and "appeared to be safe with respect to the risk of bleeding."[13] In addition to targeting FXI, the discovery of active site and allosteric inhibitors of FXIa have also garnered considerable attention.[14-24] The active site FXIa inhibitors, which are divided into irreversible and reversible inhibitors, are much more potent than the current allosteric FXIa inhibitors.[17] Active site irreversible FXIa inhibitors, represented by the previously published β-lactam[14] and α-ketothiazole peptidomimetics,[15] were found to be efficacious in both venous and arterial thrombosis animal models with little to no effect on provoked bleeding.[16] We have previously disclosed several potent, reversible FXIa inhibitors from a number of structurally diverse chemotypes which include the tetrahydroquinoline,[18] indole,[19] phenyl imidazole,[20,21] phenyl

pyridine,[22] and the phenylalanine derived diamide series.[23] Importantly, several of these inhibitors exhibited potent antithrombotic efficacy in rabbit thrombosis models with no detectable effects on cuticle bleeding.[18b,21b]

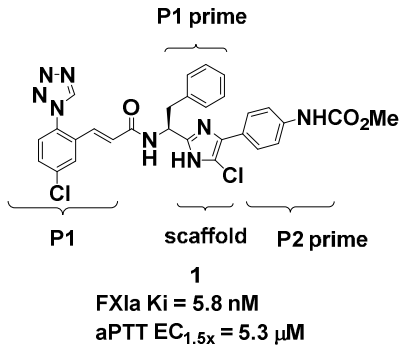

Figure 1. Imidazole-Based FXIa Inhibitors.

Extensive SAR in the phenyl imidazole series led to the discovery of **1**, a single-digit nanomolar FXIa inhibitor (FXIa Ki = 5.8 nM) with good in vitro anticoagulant activity as measured by an activated partial thromboplastin time (aPTT) clotting assay ($EC_{1.5x}$ = 5.3 μM).[21a] To address the need for additional improvements in both FXIa binding affinity and aPTT potency, we sought to preorganize the bioactive conformation of **1** via the formation of a macrocyclic ring. Macrocyclic scaffolds have been recognized as an important structural class in drug research and development demonstrating improved properties such as binding affinity, selectivity, and physicochemical properties when compared to the corresponding acyclic precursor.[25] A recent analysis by Giordanetto and Kihlberg revealed that there are currently 68 marketed macrocyclic drugs and 35 macrocycles that are in various stages of clinical development.[26] Macrocyclization strategies were successful in discovering potent inhibitors for other blood coagulation proteases such as thrombin[27] and Factor VIIa.[28] Herein we report on the discovery of a novel series of potent and selective macrocyclic FXIa inhibitors.

DESIGN OF MACROCYCLIC FXIa INHIBITORS

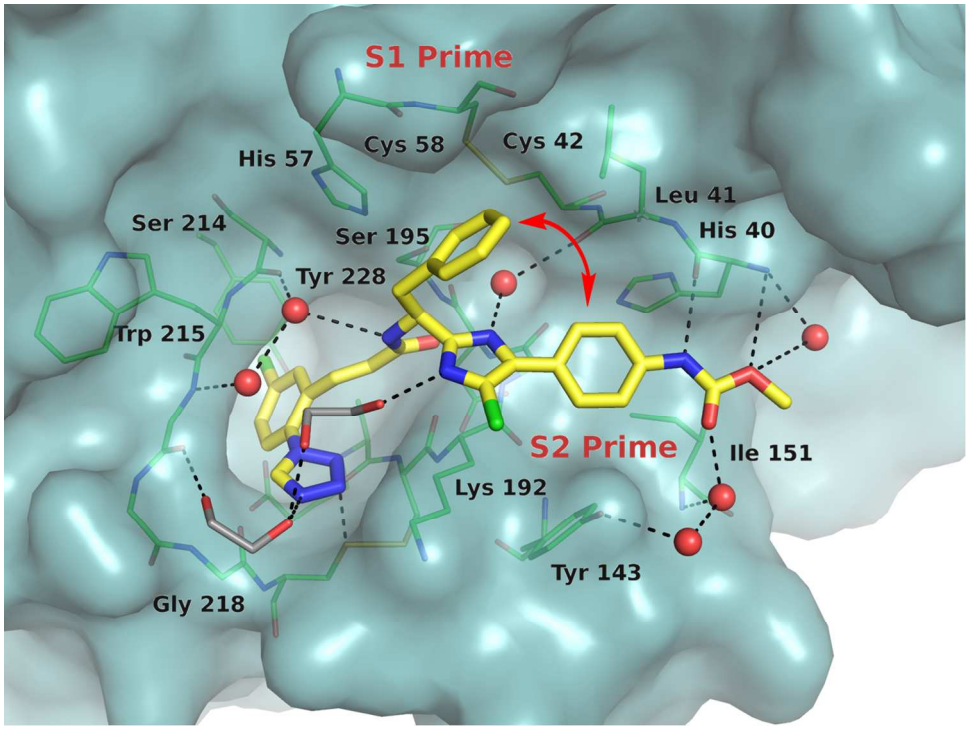

Figure 2. X-ray crystal structure of acyclic phenyl imidazole **1** in Factor XIa. The red spheres depict water molecules and the dotted lines depict hydrogen bonds. The red arrows depict the potential for macrocyclization between the P1 prime and P2 prime groups. Ethylene diol is an artifact of the flash-cooling procedure.

The X-ray crystal structure of phenyl imidazole **1** bound to FXIa (Figure 2) shows the ligand occuping the S1, S1 prime, and the S2 prime binding pockets.[21b] The p-chloro-phenyltetrazole moiety fills the S1 pocket. The benzyl moiety occupies the lipophilic S1 prime pocket with an edge-on hydrophobic interaction between the phenyl ring and the disulfide bridge Cys58-Cys42. The methyl *N*-phenyl carbamate occupies the S2 prime pocket with the carbamate forming several hydrogen bonds either directly with the enzyme or through water molecules. Owing to the close spatial proximity of the P1 prime benzyl and the P2 prime phenyl groups, we envisioned that these two groups could be linked in a favorable geometry to form a macrocyclic ring. We anticipated that preorganization of the bioactive conformation of **1**, via this macrocyclization strategy, would lead to desired improvements in FXIa potency. In

addition, the macrocyclic linker would allow further exploration of the region in the FXIa active site between the S1 prime and S2 prime pockets.

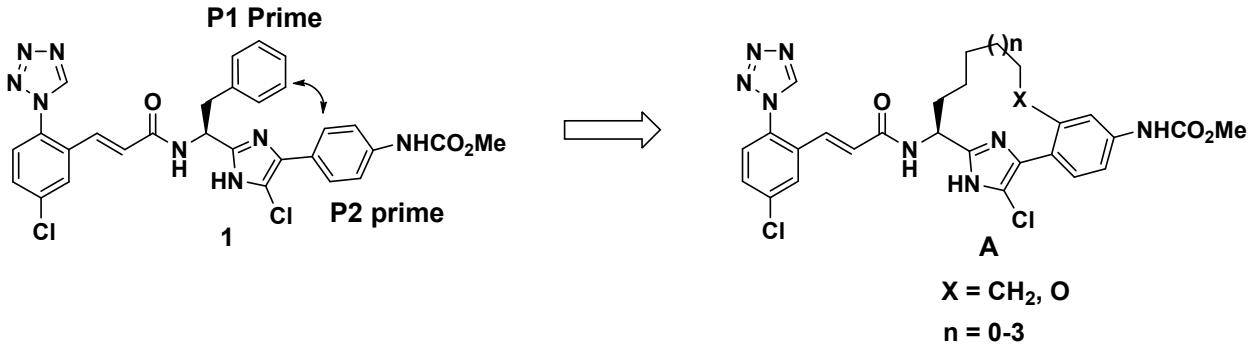

Figure 3. Macrocyclization strategy is to link the P1 prime to the ortho position of the P2 prime phenyl to form a ring.

One of our macrocyclization strategies, represented by structure A (Figure 3), removes the P1 prime phenyl and connects the P1 prime to the ortho position of the P2 prime phenyl via an alkyl or ether linker of varying lengths. We envisioned that the macrocyclic alkyl/ether linker would provide the required conformational flexibility to efficiently interact with the FXIa binding pocket. Molecular modeling was employed to help guide our initial choice of ring size. A series of medium size and macrocyclic ring structures, ranging in size from 11- to 14-membered rings, were evaluated. Truncated macrocycles, in which the P1 amide was removed, were subjected to conformational analysis using MacroModel (Schrodinger, LLC). The truncated macrocycles were used because when the entire molecule was subjected to conformational analysis, the majority of the conformations that resulted showed a hydrophobic collapse between the P1 and P2 prime regions of the molecule and did not represent realistic bioactive conformations. The conformers were overlayed on the crystal structure of acyclic phenyl imidazole **1**, superimposing the imidazole scaffolds and determining the ring sizes that may best fit into the active site. The macrocycle rings were then spliced into the crystal structure of **1** and minimized using Impact (Schrodinger, LLC) in the presence of the protein and some crystallographic waters and allowing 5 Å around the protein to flex. After minimization, ring

strain was evaluated using Jaguar (Schrodinger, LLC) DFT (B3YLP/6-31G**). The analysis showed that the 11-membered ring was too strained and could not adopt a reasonable bioactive conformation. The 14-membered ring was able to maintain conformations similar to the acyclic compound, but the additional methylene groups in the linker did not increase interactions with the protein. The 12- and 13-membered macrocyclic rings had conformations that were similar to the acyclic crystallographic conformation, without any ring strain or unnecessary methylene groups in the linker and therefore were recommended for synthesis (Please see supporting information for a more detailed conformational analysis).

CHEMISTRY

Scheme 1. Synthesis of Ring-Closing Metathesis Precursors for Alkyl- and Ether-Linked Macrocycles.[a]

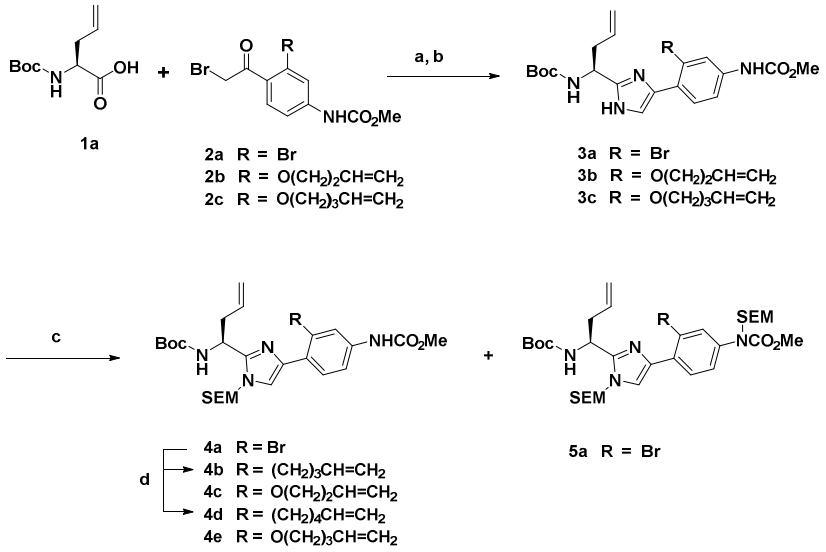

[a]Reagents and conditions: (a) $KHCO_3$, DMF, 0 °C; (b) NH_4OAc, xylene, reflux or toluene at 160 °C in microwave, 46-56% over two steps, then chiral preparatory supercritical fluid chromatography; (c) NaH, SEM-Cl, THF, 0 °C to rt, 40-51%; (d) pent-4-enyl boronic acid or hex-5-enyl boronic acid, $Pd(dppf)Cl_2 \cdot CH_2Cl_2$, K_2CO_3, Ag_2O, THF, reflux, 15-19%.

A variety of 12- and 13-membered macrocycles were prepared utilizing a ring-closing olefin metathesis (RCM) strategy.[29] The preparation of RCM precursors for the alkyl- and ether-linked macrocycles is described in Scheme 1. Alkylation of the potassium salt of **1a** with α-

bromoketone **2a** gave the corresponding keto ester intermediate. Condensation of the keto ester intermediate with NH_4OAc in xylene or toluene at elevated temperatures provided imidazole **3a**.[30] The % enantiomeric excess (% ee) of **3a**, which varied between 82 to 95% ee depending on the reaction, was improved to >99% ee by preparative supercritical fluid chromatography. Imidazole **3a** was deprotonated with NaH and then reacted with SEM-Cl which yielded a mixture of protected imidazole derivatives **4a** and **5a**. Suzuki-Miyaura coupling between **4a** and either pent-4-enyl boronic acid or hex-5-enyl boronic acid provided RCM precursors for the 12- and 13-membered alkyl-linked macrocycles **4b** and **4d**, respectively.[31] RCM precursors for the 12- and 13-membered ether-linked macrocycles **4c** and **4e** were prepared following an analogous sequence as described above for the preparation of **4a**.

Scheme 2. Synthesis of Ring-Closing Metathesis Precursors for Amide-, Carbamate, and Amine-Linked Macrocycles.[a]

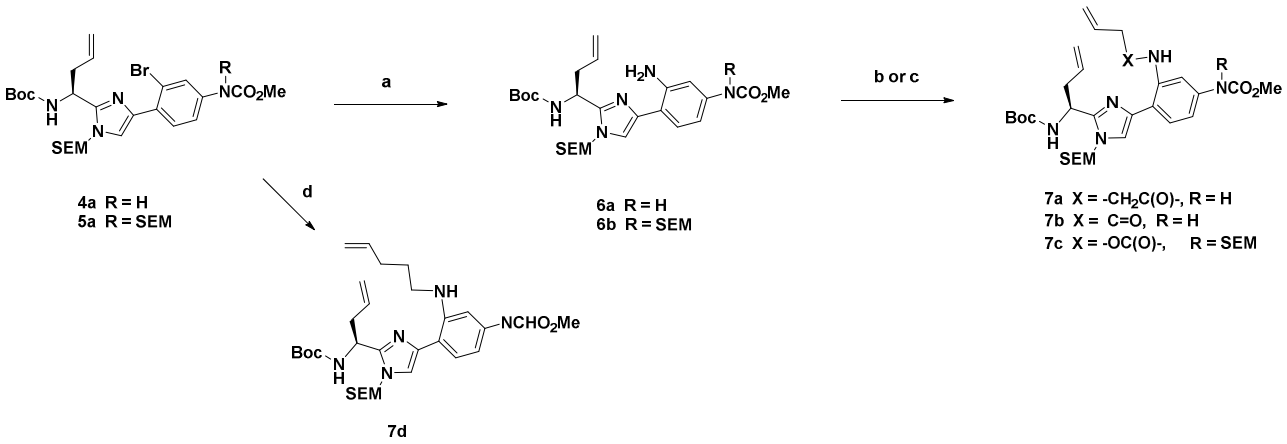

[a]Reagents and conditions: (a) NH_4OH, CuI, L-proline, K_2CO_3, DMSO, 85 °C, 59% or NaN_3, CuI, L-proline, NaOH, EtOH, 95 °C, 50%; (b) 4-pentenoic acid or 3-butenoic acid, T_3P, Hunig's base, EtOAc, -10 °C to rt, 75-87%; (c) prop-2-en-1-yl chloroformate, pyridine, DCM, 0 °C, 96%; (d) pent-4-en-1-amine, CuI, L-proline, K_2CO_3, DMSO, 90 °C, 45%.

The synthesis of RCM precursors for the amide-, carbamate-, and amine-linked macrocycles is described in Scheme 2. Amination of bromide **4a** with NH_4OH in the presence of CuI and L-proline afforded aniline **6a**.[32] Alternatively, amination of bromide **4a** with NaN_3 in the presence of CuI and L-proline, followed by in situ reduction of the azide, provided aniline **6b**.[33]

Aniline **6a** was coupled with 4-pentenoic acid or 3-butenoic acid using T_3P which gave amides **7a** and **7b**, respectively. Carbamate **7c** was prepared by reacting aniline **6b** with prop-2-en-1-yl chloroformate. Bromide **4a** was coupled with pent-4-en-1-amine using CuI which provided substituted aniline **7d**.

Scheme 3. Synthesis of 12- and 13-Membered Alkyl- and Ether-Linked Macrocycles **2**-**12**.[a]

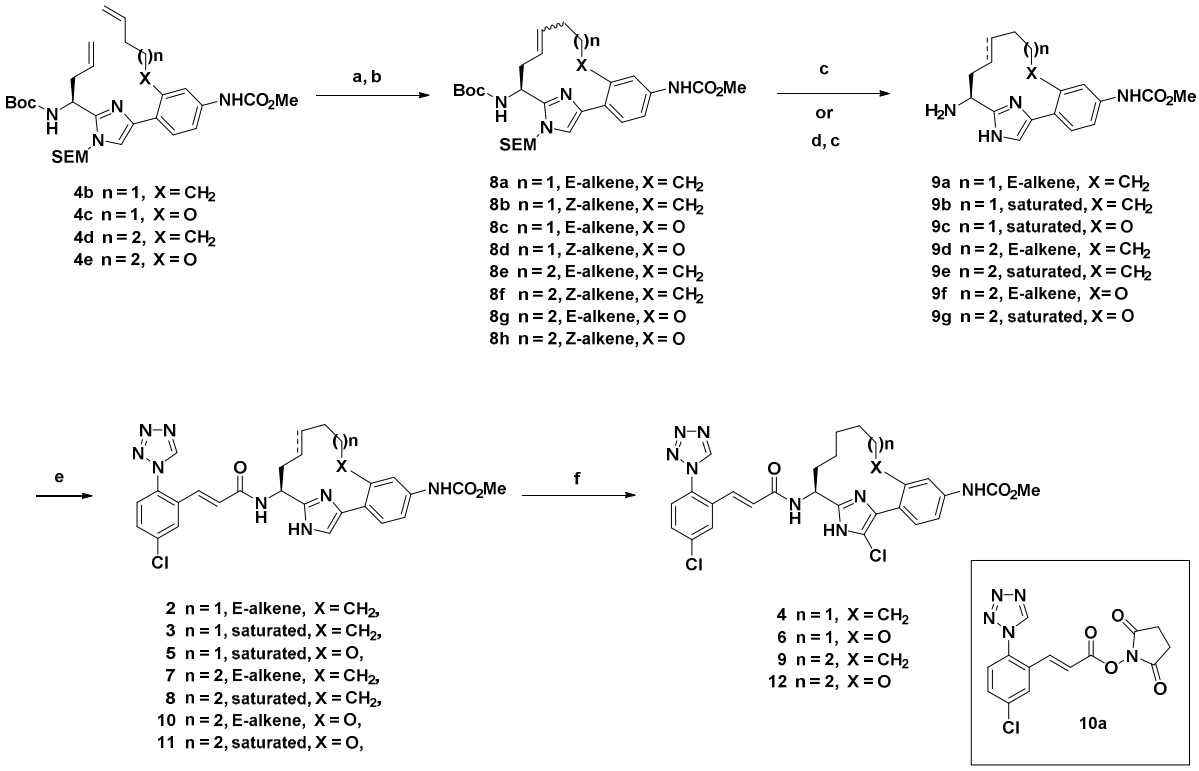

[a]Reagents and conditions: (a) Second generation Grubbs II catalyst (40 mol%), *p*TsOH, DCM, reflux; (b) preparatory HPLC to separate E/Z-alkene isomers: 52% for **8a**:**8b** (3.6:1), 38% for **8c**:**8d** (2.2:1), 63% for **8e**:**8f** (1:1.7), 58% for **8g**:**8h** (1:1.3); (c) 5M HCl (aq), MeOH, 75 °C, 75-94%; (d) 10% Pd/C, H_2, MeOH, 38-78% over two steps; (e) **10a**, Hunig's base, DMF, 26-91%; (f) NCS, ACN, $CHCl_3$, with or without Hunig's base, 65 °C, 31-59%.

The synthesis of the 12- and 13-membered alkyl- and ether-linked macrocycles **2**-**12** is described in Scheme 3. Using a modified procedure described by Lovely,[34] **4b** was pretreated with p-TsOH to form the imidazolium ion and then cyclized via ring-closing metathesis using the second generation Grubbs (II) catalyst in refluxing DCM to give the 12-membered alkyl-linked

macrocycle as a 3.6:1 mixture of E-alkene **8a** and Z-alkene **8b** isomers. The E/Z-alkene isomers were separated by reverse phase chromatography. The geometry of the alkene bond was determined by ^{1}H-^{1}H-homonuclear decoupling of the two sets of vicinal methylene protons which revealed the *J* coupling constant between the double bond protons; the E-alkene exhibiting a *J*

coupling = ~15 Hz and the Z-alkene exhibiting a *J* coupling = ~10.5 Hz. Deprotection of both Boc and SEM groups with aqueous 5 M HCl in MeOH at 75 °C afforded the unsaturated macrocyclic amine **9a**. Hydrogenation of the E/Z-alkene mixture **8a** and **8b** over palladium on carbon, followed by deprotection as described above for **9a**, yielded the saturated macrocyclic amine **9b**. The p-chlorophenyltetrazole cinnamide P1 was installed by coupling amines **9a** and **9b** with the activated carboxylic ester **10a** which gave amides **2** and **3**. Chlorination of **2** with NCS at elevated temperature provided chloro-imidazole **4**. In a similar fashion, RCM precursors **4c**-**4e** were converted to their corresponding 12- and 13-membered alkyl- and ether-linked macrocycles **5**-**12**.

Scheme 4. Synthesis of 13-Membered Amide-, Carbamate-, and Amine-Linked Macrocycles **13**-**20**.[a]

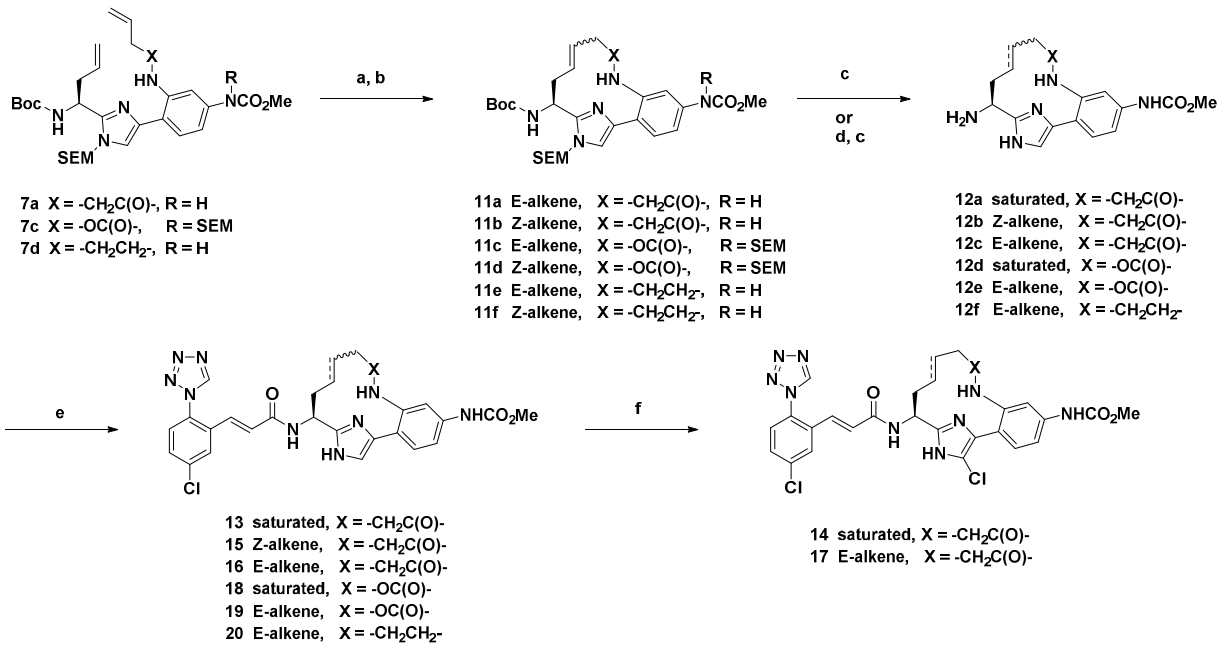

[a]Reagents and conditions: (a) Second generation Grubbs II catalyst (5 to 40 mol%), *p*TsOH, DCM, reflux; (b) preparatory HPLC or normal phase chromatography to separate E/Z-alkene isomers: 76% for **11a**:**11b** (1.4:1 E:Z), 74% for **11c**:**11d** (4.7:1 E:Z), 89% for **11e**:**11f** (1:4.2 E:Z); (c) 5M HCl (aq), MeOH, 75 °C; or 4M HCl in dioxane, 75 °C, 46-98%; (d) 10% Pd/C, H_2, MeOH or EtOAc; (e) **10a**, Hunig's base, DMF, 13-54%; (f) NCS, ACN, $CHCl_3$, 65 °C, 41-44%.

Scheme 4 describes the synthesis of the 13-membered amide-, carbamate-, and amine-linked macrocycles **13**-**20** and Scheme 5 describes the synthesis of the 12-membered amide-linked macrocycles **22** and **23**. These macrocycles were synthesized from RCM precursors **7a**-**7d** using an analogous sequence to that described for the preparation of macrocycles **2**-**4**.

Scheme 5. Synthesis of 12-Membered Saturated Amide- and Unsaturated Amide-Linked Macrocycles **22** and **23**.[a]

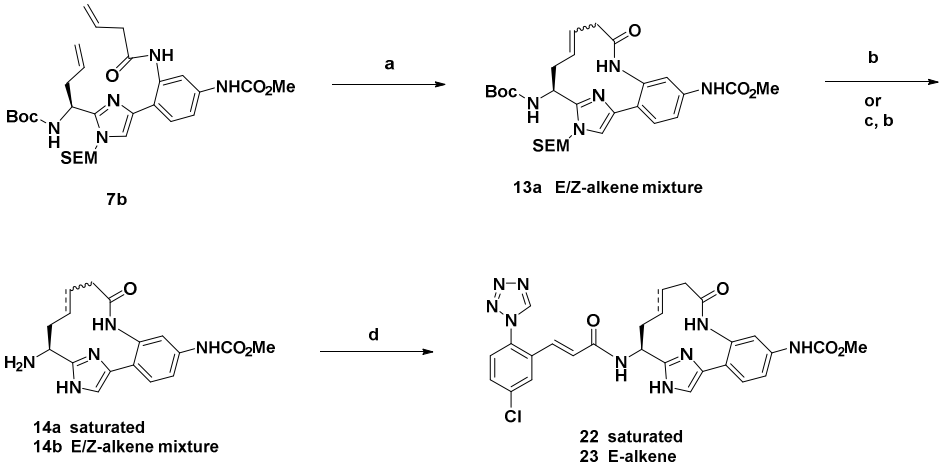

[a]Reagents and conditions: (a) Second generation Grubbs II catalyst (40 mol%), *p*TsOH, DCM, reflux, 66% for **13a** (2.2:1 E:Z); (b) 4M HCl in dioxane, 50 °C, 74-82%; (c) 10% Pd/C, H_2, MeOH, EtOAc; (d) **10a**, Hunig's base, DMF, 27-37% over two steps.

RESULTS AND DISCUSSION

Our initial survey of macrocyclic FXIa inhibitors focused on 12- and 13-membered alkyl- and ether-linked macrocycles (Table 1). Even though we were particularly interested in the saturated alkyl/ether linked macrocycles represented by structure A (Figure 3), we also assayed the unsaturated linkers since they were available from the RCM chemistry. Macrocycle **2**, the 12-membered ring possessing the E-alkene, showed a significant loss in FXIa activity (FXIa Ki = 636 nM) compared to acyclic phenyl imidazole **1** (FXIa Ki = 5.8 nM).[35] Removing the unsaturation from the macrocyclic linker gave the saturated alkyl linker **3** (FXIa Ki = 87 nM) which improved FXIa activity by 7-fold. We had previously discovered in the acyclic series that chlorination of the imidazole scaffold would provide a 5 to 10-fold increase in FXIa activity; however, only a modest 2-fold increase in FXIa activity was observed with chloro-imidazole **4** (FXIa Ki = 42 nM).[20] The 12-membered ether-linked macrocycles **5** and **6** were much less potent than their corresponding alkyl-linked derivatives **3** and **4**. In contrast to the SAR trends in the 12-membered alkyl macrocycles, the 13-membered macrocycle **7**, possessing the unsaturated alkyl-linker, was more potent than the saturated alkyl macrocycle **8**. In addition, the chloro-imidazole in the 13-membered alkyl linker **9** (FXIa Ki = 68 nM) resulted in an 8-fold increase in FXIa activity. The 13-membered ether-linked macrocycles **11** and **12** were either slightly improved or equipotent to their corresponding alkyl-linked derivatives **8** and **9**. The most potent macrocycles identified from our initial survey, analogs **4**, **9**, and **12**, were approximately an order of magnitude less potent than acyclic phenyl imidazole **1**.

Table 1. 12- and 13-Membered Alkyl- and Ether-Linked Macrocycles

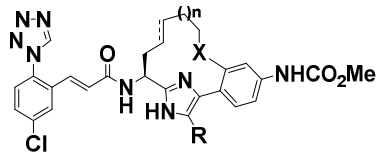

Entry	Alkene	n	Ring Size	X	R	FXIa Ki[a] (nM)	aPTT[b] $EC_{1.5x}$ (μM)
1	--	--	--	--	--	5.8	5.3
2	E-alkene	1	12	CH_2	H	636[c]	NT[d]
3	Saturated	1	12	CH_2	H	87	>40
4	Saturated	1	12	CH_2	Cl	42	27
5	Saturated	1	12	O	H	420[c]	NT[d]
6	Saturated	1	12	O	Cl	250[c]	NT[d]
7	E-alkene	2	13	CH_2	H	184	>40
8	Saturated	2	13	CH_2	H	600	NT[d]
9	Saturated	2	13	CH_2	Cl	68	34
10	E-alkene	2	13	O	H	3,920	NT[d]
11	Saturated	2	13	O	H	159	NT[d]
12	Saturated	2	13	O	Cl	76	>40

[a]Ki values were obtained from purified human enzyme at 37 °C and were averaged from multiple determinations (n=2), as described in Ref. 18a. [b]aPTT (activated partial thromboplastin time) in vitro clotting assay was performed in human plasma. [c]Ki values were determined at 25 °C. [d]NT = Not tested.

In order to better understand how these macrocycles bind in the active site of FXIa, an X-ray crystal structure of the 13-membered macrocycle **9** bound to FXIa (1.6 Å resolution, R-work was 0.160 and R-free was 0.176, Figure 4) was obtained. An overlay of macrocycle **9** with acyclic phenyl imidazole **1** (Figure 5) revealed conformation changes in the macrocycle which may explain the loss in FXIa activity. The benzylic carbon of the P2 prime phenyl, which is part of the macrocyclic linker, is in close spatial proximity (3.2 Å) to the carbonyl of Leu41. In order to minimize the steric clash between these two groups, the P2 prime phenyl rotates 28° which

increases the dihedral angle in the macrocycle compared to acyclic phenyl imidazole **1** (Figure 5B; dihedral angle of P2 prime phenyl was 53° for **9** and 25° for **1**).[36] The larger dihedral angle of the P2 prime phenyl does not appear to affect the key hydrogen bonding interactions of the

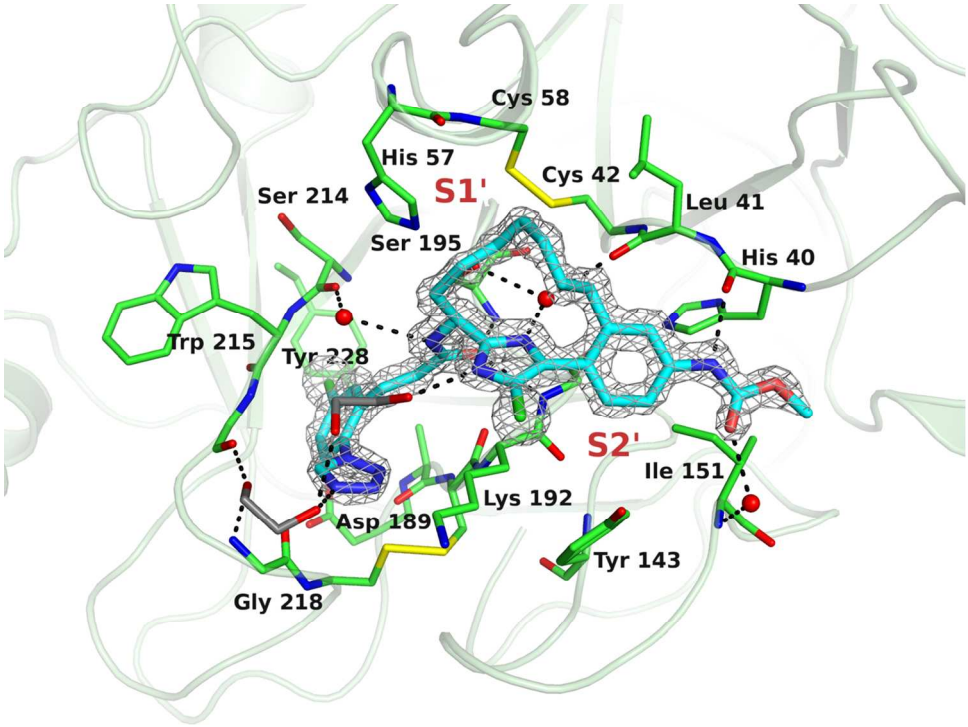

Figure 4. X-ray crystal structure of 13-membered macrocycle **9** bound to Factor XIa with omit mFo-DFc electron density contoured at 5 r.m.s.d (gray). The red spheres depict water molecules and the dotted lines depict hydrogen bonds. Ethylene diol is an artifact of the flash-cooling procedure.

carbamate moiety[37] but it pulls the macrocyclic linker out of the S1 prime pocket minimizing the interaction with the lipophilic region.[38] The X-ray crystal structure of **9** can explain the SAR trends observed with the 12- and 13-membered ether-linked macrocycles. The ether-linked macrocycles have an oxygen atom in close spatial proximity to the carbonyl of Leu41. For the 12-membered macrocycles **5** and **6**, the electrostatic repulsion between the oxygen atom in the macrocyclic linker and the carbonyl of Leu41 leads to a loss in FXIa activity. What is interesting however, was the finding that the 13-membered ether-linked macrocycles **11** and **12** did not show a loss in FXIa activity compared to their alkyl-linked analogs **8** and **9**. It is postulated that

the additional methylene in the linker provides enough flexibility whereby the linker can adopt a conformation which minimizes the electrostatic repulsion. However, when unsaturation was present in the macrocyclic linker, as in **10**, this conformational flexibility was lost and the electrostatic repulsion could not be minimized which resulted in a weak FXIa inhibitor (FXIa Ki = 3,920 nM).

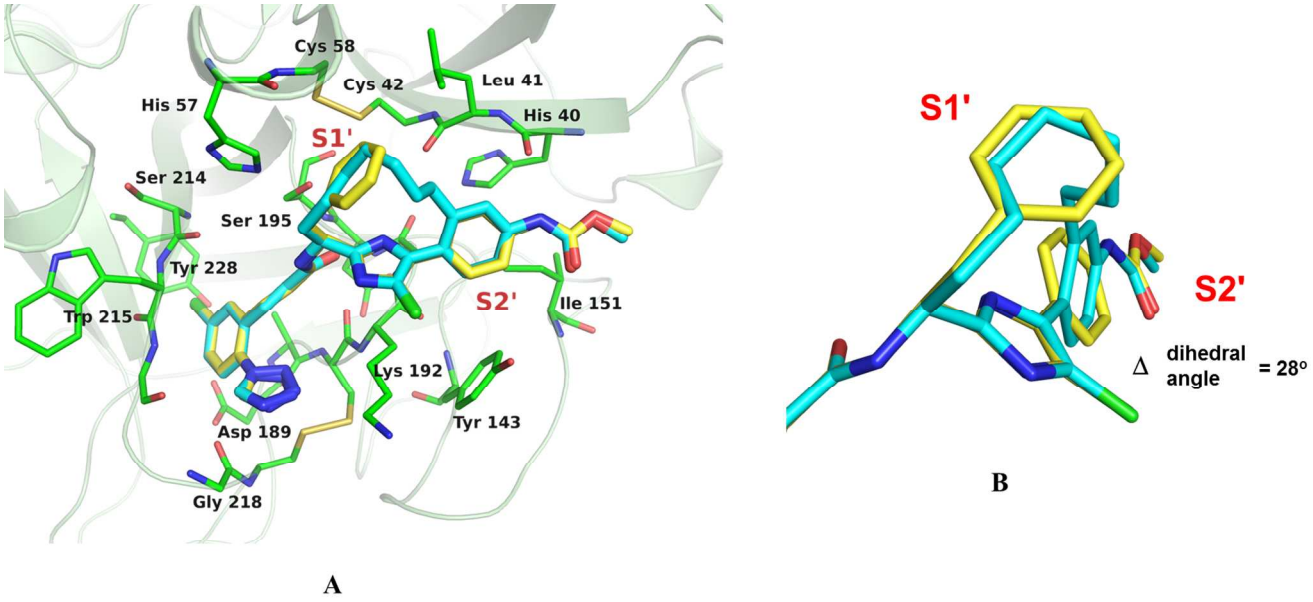

Figure 5. (A) Overlay of X-ray crystal structures of acyclic phenyl imidazole **1** (yellow) and 13-membered macrocycle **9** (cyan) in Factor XIa. (B) Overlay of X-ray crystal structures of acyclic phenyl imidazole **1** (yellow) and 13-membered macrocycle **9** (cyan) in Factor XIa looking into the S2 prime pocket. The increased dihedral angle in macrocycle **9** pulled the macrocyclic linker out of the S1 prime pocket.

Owing to the close spatial proximity of the benzylic carbon of the macrocyclic linker in **9** to the carbonyl of Leu41, we envisioned that introduction of an amide N-H in the linker would improve the FXIa activity via a hydrogen bonding interaction. Indeed, incorporation of the amide moiety into the 13-membered macrocycle had a profound impact on both FXIa binding affinity and potency in the aPTT clotting assay (Table 2). Specifically, the saturated amide linker **13** (FXIa Ki = 3.2 nM; aPTT = 1.2 μM) was a single-digit nanomolar FXIa inhibitor with good activity in the aPTT clotting assay. Furthermore, chloro-imidazole **14** led to a 6 to 7-fold increase in FXIa activity (FXIa Ki = 0.47 nM) but with only a modest improvement in the aPTT

clotting activity; however in vitro human liver microsome (HLM) $T_{1/2}$ was improved compared to **13**. Importantly, comparing macrocycle **14** with acyclic phenyl imidazole **1**, the macrocyclic analog improved FXIa

Table 2. 13-Membered Amide, Carbamate, and Amine-Linked Macrocycles

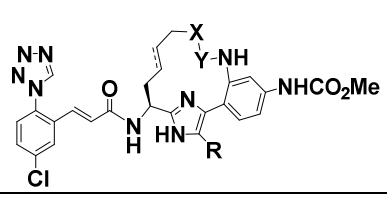

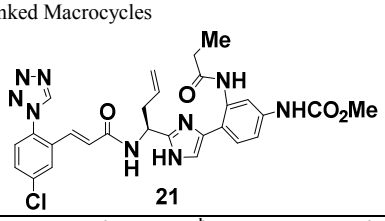

21

Entry	Alkene	X	Y	R	FXIa Ki[a] (nM)	aPTT[b] $EC_{1.5x}$ (μM)	HLM[c] $T_{1/2}$ (min.)
13	**Saturated**	**CH_2**	**C=O**	**H**	**3.2**	**1.2**	**34**
14	**Saturated**	**CH_2**	**C=O**	**Cl**	**0.47**	**0.92**	**86**
15	**Z-alkene**	**CH_2**	**C=O**	**H**	**5.2**	**12**	**NT[e]**
16	**E-alkene**	**CH_2**	**C=O**	**H**	**0.16**	**0.27**	**41**
17	**E-alkene**	**CH_2**	**C=O**	**Cl**	**0.03**	**0.28**	**58**
18	**Saturated**	**O**	**C=O**	**H**	**3.8**	**0.86**	**62**
19	**E-alkene**	**O**	**C=O**	**H**	**0.88**	**0.45**	**69**
20	**E-alkene**	**CH_2**	**CH_2**	**H**	**514**	**NT[d]**	**17**
21	**--**	**--**	**--**	**--**	**27**	**21**	**12**

[a]Ki values were obtained from purified human enzyme at 37 °C and were averaged from multiple determinations (n=2), as described in Ref. 18a. [b]aPTT (activated partial thromboplastin time) in vitro clotting assay was performed in human plasma. [c]HLM = human liver microsome stability. [d]NT = Not tested

affinity by 10-fold and aPTT potency by 5-fold. Though the Z-alkene amide macrocycle **15** was less potent than the saturated amide linker **13**, the E-alkene amide macrocycle **16** had a FXIa Ki = 0.16 nM with potent anticoagulant activity in the in vitro clotting assay (aPTT $EC_{1.5x}$ = 0.27 μM). The corresponding chloro-imidazole **17** further improved the FXIa affinity with a FXIa Ki = 0.03 nM however the potency in the clotting assay was unchanged. Next, we examined other

NH bond donors at the benzylic position of the macrocyclic linker. The saturated carbamate linker **18** was equipotent to the saturated amide linker **13**. Even though the unsaturated carbamate linker **19** was 5 to 6-fold less potent than the corresponding amide **16**, it was still a sub-nanomolar FXIa inhibitor. The type of NH bond donor at the benzylic position was critical for FXIa affinity, the amide-linked macrocycle **16** was >1,000-fold more potent than the amine-linked macrocycle **20**.[39] We went back to evaluate installation of the amide moiety in the acyclic series to determine whether similar potency enhancements could be achieved. However, this was not the case, as acyclic analog **21** resulted in a 160-fold loss in FXIa activity compared to macrocycle **16**.

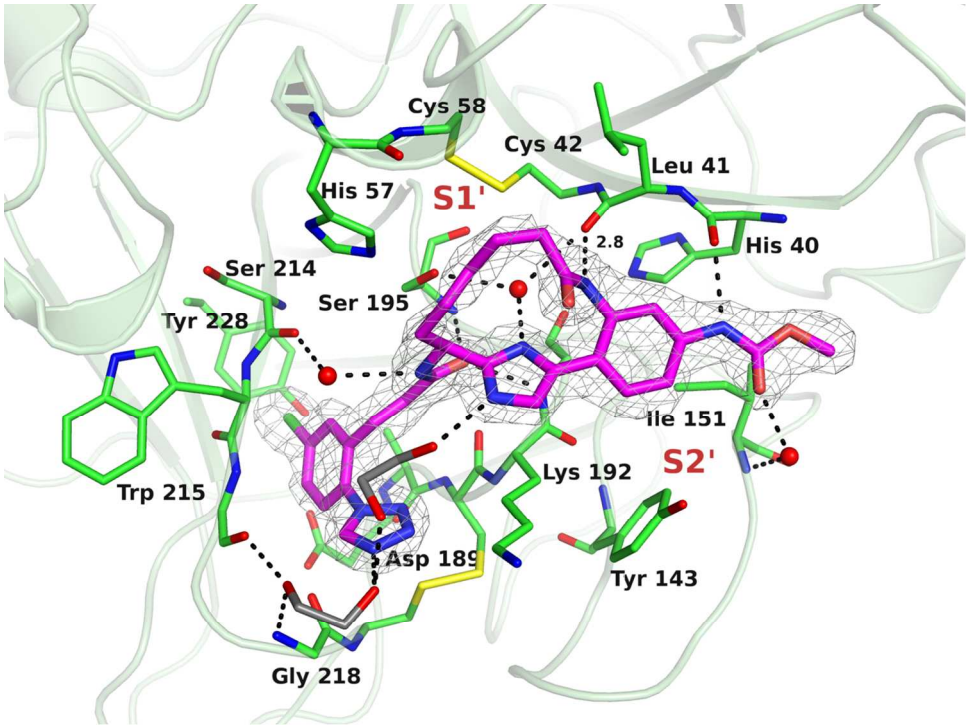

Figure 6. X-ray crystal structure of 13-membered unsaturated amide-linked macrocycle **16** bound to Factor XIa with omit mFo-DFc electron density contoured at 3.5 r.m.s.d (gray). The red spheres depict water molecules and the dotted lines depict hydrogen bonds. Ethylene diol is an artifact of the flash-cooling procedure.

An X-ray crystal structure of the 13-membered unsaturated amide-linked macrocycle **16** bound to FXIa (2.1 Å resolution, R-work was 0.170 and R-free was 0.192 , Figure 6) was obtained and it confirmed the key hydrogen bonding interaction between the amide NH in the

macrocyclic linker and the carbonyl of Leu41 (2.8 Å). The macrocyclic linker was critical in orienting the amide NH in an ideal position to form a strong hydrogen bonding interaction. Even though the dihedral angle of the P2 prime phenyl in **16** (∠ = 43°) is smaller than the alkyl-linked macrocycle **9** (∠ = 53°), the macrocyclic linker is still pulled away from the S1 prime pocket preventing van der Waals contact with the S1 prime disulfide bridge.[40] As the result, the 20-fold increase in FXIa activity that was seen with incorporation of E-alkene into the macrocyclic linker **16**, compared to the saturated macrocyclic linker **13** (Figures S1 and S2 in supporting information), was most likely due to conformation entropy.

Table 3. 12- and 13-Membered Saturated and Unsaturated Amide-Linked Macrocycles

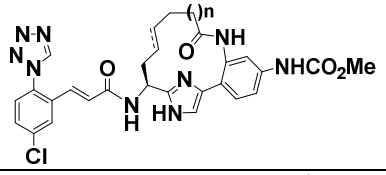

Entry	Alkene	n	Ring Size	FXIa Ki[a] (nM)	aPTT[b] $EC_{1.5x}$ (μM)	HLM[c] $T_{1/2}$ (min.)
22	**Saturated**	**0**	**12**	**1.0**	**0.30**	**90**
13	**Saturated**	**1**	**13**	**3.2**	**1.2**	**34**
23	**E-alkene**	**0**	**12**	**264**	**>40**	**NT[d]**
16	**E-alkene**	**1**	**13**	**0.16**	**0.27**	**41**

[a]Ki values were obtained from purified human enzyme at 37 °C and were averaged from multiple determinations (n=2), as described in Ref. 18a. [b]aPTT (activated partial thromboplastin time) in vitro clotting assay was performed in human plasma. [c]HLM = human liver microsome stability. [d]NT = Not tested.

With the discovery of the macrocyclic amide linker in the 13-membered macrocycle we shifted our focus to the 12-membered macrocycle. Both the saturated amide linker and the unsaturated amide linker were incorporated in the 12-membered ring system (Table 3) and compared to the 13-membered ring system. The 12-membered macrocycle **22** containing the saturated amide linker resulted in a 3-fold improvement in FXIa affinity and a 4-fold improvement in the aPTT clotting assay compared to the 13-membered macrocycle **13**. The

HLM stability for **22** ($T_{1/2}$ = 90 min) was also improved compared to **13** ($T_{1/2}$ = 34 min). Based on FXIa potency and HLM stability, the 12-membered ring system was preferred for the saturated amide linker. In contrast, the 13-membered ring system was preferred for the unsaturated amide linker as the 12-membered ring **23** resulted in a significant loss in potency. Molecular modeling indicated that the loss in potency with the 12-membered macrocycle **23** was due to ring strain which prevented the amide moiety from adopting the preferred orientation to participate in the key hydrogen bond with the carbonyl of Leu41.

Pharmacokinetic Profiles. The pharmacokinetic profile for several macrocyclic compounds were evaluated in dog, using an N-in-one cassette dosing protocol (Table 4).[41] The 12-membered alkyl-linked macrocycle **3** exhibited a low clearance, a moderate half-life, and modest oral bioavailability in dog (%F = 12). Introduction of the amide moiety into the 12-membered macrocyclic linker **22** increased the clearance, shortened the half-life and significantly reduced the oral exposure (**3**: AUC = 458 nM*h versus **22**: AUC = 21 nM*h). The 13-membered ether-linked macrocycle **11** exhibited a moderate clearance and showed modest oral bioavailability (%F = 17). Similar to what was observed for the 12-membered macrocycles, the 13-membered amide linked macrocycles **13** and **16** showed high clearance, a short half-life, and were not orally bioavailable. The amide moiety, which led to a significant improvement in terms of both FXIa activity and potency in the aPTT clotting assay, was deleterious for oral bioavailability. The poor oral bioavailability of the amide-linked macrocycles was attributed to the low permeability (Caco-2 A to B < 15 nm/sec) arising from the high polar surface area (169 Å^2).

Table 4. Pharmacokinetic Profile In Dog For Selected Macrocycles.

Entry	Cl[a] (mL/h/kg)	$T_{1/2}$ (h)	Vdss (L/kg)	F (%)	AUC (nM*h)	Dose iv/po (mpk)	DLM[d] $T_{1/2}$ (min)	Dog Protein Binding (% bound)
3	**2.6**	**3.2**	**0.7**	**12**	**458[b]**	**0.21/0.42**	**>120**	**NT[e]**
22	**15**	**1.0**	**0.8**	**6**	**21[c]**	**0.20/0.23**	**>120**	**90.2**

11	**13**	**2.1**	**2.2**	**17**	**119**[b]	**0.20/0.40**	**88**	**NT**[e]
13	**68**	**1.1**	**3.9**	**0**	**0**[b]	**0.20/0.35**	**>120**	**93.4**
16	**23**	**1.2**	**1.8**	**1**	**2.5**[c]	**0.19/0.32**	**>120**	**91.5**

[a]Compounds were dosed in dog in an *N*-in-1 format. [b]Vehicle for iv: 70% PEG 400; 20% water; 10% ethanol. Vehicle for po: 70% PEG 400; 20% TPGS; 10% ethanol. [c]Vehicle for both iv and po: 70% PEG 400; 20% water; 10% ethanol. [d]DLM = dog liver microsome stability. [e]NT = Not tested

Serine Protease Selectivity. The 13-membered unsaturated amide-linked macrocycle **16** and the 12-membered saturated amide-linked macrocycle **22** were tested against a panel of relevant serine proteases including the blood coagulation proteases (Table 5). For comparison, acyclic phenyl imidazole **1** is included. Similar to the acyclic phenyl imidazole **1**, the macrocycles **16** and **22** showed >1,000-fold selectivity against many of the relevant proteases, except for plasma kallikrein (70 to 100-fold).[42]

Table 5. Human Serine Protease Selectivity Profile for **1**, **16**, and **22**.

Human Enzyme Ki (nM)[a]	**1**	**16**	**22**
Factor XIa	**5.8**	**0.16**	**1.0**
Factor VIIa[b]	**>13,400**	**1,670**	**3,190**
Factor IXa	**>27,100**	**>27,100**	**>27,100**
Factor Xa	**>13,300**	**>13,300**	**>13,300**
Factor XIIa	**>3,050**	**>3,050**	**>3,050**
Thrombin	**>11,500**	**>11,500**	**>11,500**
Trypsin	**>10,000**	**1,520**	**8,390**
Plasma Kallikrein	**519**	**16**	**70**
Activated Protein C	**>21,500**	**>21,500**	**>21,500**
Plasmin	**>15,200**	**>14,200**	**>15,200**
TPA	**>6,150**	**>6,150**	**>6,150**
Urokinase	**>15,100**	**5,050**	**>15,100**
Chymotrypsin	**>4,530**	**1,500**	**3,940**

[a]K_i values in nM were obtained using human purified enzymes at 37 °C. [b]K_i values in nM were obtained using human purified enzymes at 25 °C.

CONCLUSION

A novel series of macrocyclic FXIa inhibitors was designed based on the X-ray crystal structure of the acyclic phenyl imidazole **1**. Our initial macrocycles, which were double-digit nanomolar FXIa inhibitors, were further optimized by structure-based drug design. This effort resulted in the discovery a macrocyclic amide linker which led to picomolar FXIa inhibitors with excellent potency in the aPTT clotting assay and greater than a 1,000-fold selectivity against the relevant blood coagulation enzymes. As an example, the 13-membered unsaturated amide-linked macrocycle **16** is a 0.16 nM inhibitor of FXIa with potent anticoagulant activity in an in vitro clotting assay (aPTT $EC_{1.5x}$ = 0.27 μM). While the macrocyclic amide linker was critical for FXIa potency, it also contributed to the poor pharmacokinetic profile. The optimization of macrocyclic FXIa inhibitors to address the poor oral bioavailability will be reported in due course.

EXPERIMENTAL SECTION

General Chemistry Methods. All reactions were carried out using commercial grade reagents and solvents. Solution ratios express a volume relationship, unless stated otherwise. NMR chemical shifts (δ) are reported in parts per million relative to internal TMS. Normal phase chromatography was carried out on ISCO CombiFlash systems using prepacked silica cartridges and eluted with gradients of the specified solvents. Preparative reverse phase high pressure liquid chromatography (HPLC) was carried out on C18 HPLC columns using methanol/water gradients containing 0.1% trifluoroacetic acid unless otherwise stated. Purity of all final compounds was determined to be ≥95% by analytical HPLC using the following conditions: SunFire C18 column (3.5 μm C18, 3.0 x 150 mm); Gradient elution (0.5 mL/min) from 10-100% Solvent B for 12 min and then 100% Solvent B for 3 min. Solvent A is (95% water, 5%

acetonitrile, 0.05% TFA) and Solvent B is (5% water, 95% acetonitrile, 0.05% TFA); monitoring UV absorbance at 220 and 254 nm.

Methyl *N*-[(11*E*,14*S*)-14-[(2*E*)-3-[5-chloro-2-(1H-1,2,3,4-tetrazol-1-yl)phenyl]prop- 2-enamido]-16,18-diazatricyclo[13.2.1.0^{2,7}]octadeca-1(17),2,4,6,11,15(18)-hexaen-5-yl]-carbamate, trifluoroacetic acid salt (2). A cloudy suspension of **9a** (0.014 g, 0.043 mmol) and (*E*)-2,5-dioxopyrrolidin-1-yl 3-(5-chloro-2-(1H-tetrazol-1-yl)phenyl)acrylate **10a**[22b] (0.015 g, 0.043 mmol) in DMF (0.43 mL) and Hunig's base (0.037 mL, 0.214 mmol) was stirred at rt. After 1.5 h, the reaction was partitioned between water and EtOAc and then the layers were separated. The aqueous layer was extracted with EtOAc (1x). The organic layers were combined and washed with sat. $NaHCO_3$, brine, dried over Na_2SO_4, filtered and concentrated to give a pale, yellow foam weighing 0.032 g. Purification by reverse phase chromatography gave after concentration and lyophilization **2** (0.0131 g, 45% over two steps) as a white solid. MS (ESI) *m/z*: 559.1 $(M+H)^+$ and 561.1 $(M+2+H)^+$. ^{1}H NMR (500 MHz, CD_3OD, 50 °C) δ ppm 9.47 (s, 1H), 7.94-7.98 (m, 1H), 7.65-7.71 (m, 1H), 7.58 (d, *J*=8.25 Hz, 1H), 7.46 (br. s, 1H), 7.37-7.41 (m, 1H), 7.29-7.37 (m, 2H), 7.19 (d, *J*=15.4 Hz, 1H), 6.76 (d, *J*=15.4 Hz, 1H), 5.50-5.60 (m, 1H), 5.09-5.19 (m, 1H), 5.02-5.09 (m, 1H), 3.75 (s, 3H), 2.77-2.86 (m, 1H), 2.40-2.60 (m, 3H), 1.95-2.05 (m, 1H), 1.85-1.95 (m, 1H), 1.49-1.62 (m, 1H), 1.25-1.38 (m, 1H). Note: proton decoupling confirmed the E-alkene geometry with a *J* coupling = 15.4 Hz.

Methyl N-[(14S)-14-[(2E)-3-[5-chloro-2-(1H-1,2,3,4-tetrazol-1-yl)phenyl]prop-2- enamido]-16,18-diazatricyclo[13.2.1.0^{2,7}]octadeca-1(17),2,4,6,15(18)-pentaen-5-yl]-carbamate, 1 tri-fluoroacetic acid salt (3). Using a procedure analogous to that which was used to prepare **2**, **9b** (0.058 g, 0.10 mmol) was coupled to **10a** to give **3** (0.044 g, 62%) as a white solid. MS (ESI)

m/z: 561.1 $(M+H)^+$. ^1H NMR (500 MHz, CD_3OD, 50 °C) δ ppm 9.47 (s, 1 H), 7.95 (d, *J*=2.2 Hz, 1 H), 7.67 (dd, *J*=8.8, 2.2 Hz, 1H), 7.57 (d, *J*=8.2 Hz, 1H), 7.46 (d, *J*=2.2 Hz, 1H), 7.41 - 7.44 (m, 2 H), 7.37 (d, *J*=8.3 Hz, 1 H), 7.17 (d, *J*=15.9 Hz, 1 H), 6.77 (d, *J*=15.9 Hz, 1 H), 5.01 (dd, *J*=9.1, 5.8 Hz, 1 H), 3.75 (s, 3 H), 2.47 - 2.56 (m, 1 H), 2.36 - 2.44 (m, 1 H), 2.17 - 2.25 (m, 1 H), 1.82 - 1.91 (m, 1 H), 1.31 - 1.56 (m, 4 H), 1.23-1.26 (m, 2 H), 0.87 - 0.98 (m, 1 H), 0.38-0.53 (m, 1 H).

***tert*-Butyl *N*-[(1*S*)-1-(4-{2-bromo-4-[(methoxycarbonyl)amino]phenyl}-1H-imidazol- 2-yl)but-3-en-1-yl]carbamate (3a)**. To a clear, colorless solution of **1a** (3.89 g, 18.1 mmol) in DMF (45.2 mL) was added $KHCO_3$ (2.17 g, 21.7 mmol). The reaction was stirred at rt for 20 min and then the reaction was cooled to 0 °C. Next a clear, yellow solution of **2a** (6.34 g, 18.1 mmol) in DMF (20 mL) was added dropwise. The reaction was stirred at 0 °C for 30 min and then the reaction was warmed to rt and stirred overnight. The reaction was cooled to 0 °C, poured into ice-cold water (200 mL) to give a white suspension and then extracted with EtOAc (3x). The organic layers were combined, washed with water (1x), brine (1x), dried over Na_2SO_4, filtered and concentrated to give 2-{2-bromo-4-[(methoxycarbonyl)-amino]phenyl}-2-oxoethyl (2*S*)-2-{[(*tert*-butoxy)carbonyl]amino}pent-4-enoate (10.26 g) as a clear, yellow oil which was used in the next reaction without further purification. MS (ESI) *m/z*: 387.0 $(M-C_5H_8O_2+2+H)^+$.

To a clear, yellow solution of 2-{2-bromo-4-[(methoxycarbonyl)-amino]phenyl}-2-oxoethyl (2*S*)-2-{[(*tert*-butoxy)carbonyl]amino}pent-4-enoate (8.77 g, 18.07 mmol) in xylene (181 mL) was added NH_4OAc (13.93 g, 181 mmol). The flask was equipped with a Dean-stark trap and a reflux condenser. The reaction was warmed to 140 ^oC. After 3 h, the reaction was cooled to rt, diluted with EtOAc (400 mL), washed with 1.5 M K_3PO_4 (2 x 150 mL), brine, dried over Na_2SO_4, filtered, and concentrated to give a brown foam. Purification by normal phase

chromatography (gradient elution 0-60% EtOAc/Hex) gave **3a** (4.61 g, 55%) as a pale, orange solid. The % enantiomeric excess (% ee) of **3a** varied (82 to 95% ee) between reactions. The % ee was further improved to >99% ee by preparative supercritical fluid chromatography (SFC) using the following conditions: Chiralcel OD-H (3 x 25 cm, Chiral Technologies, Inc.), 25% MeOH in CO_2, 110 mL/min, 35 °C, and UV detection at 240 nm. The analytical SFC conditions were the following: Chiralcel OD-H (0.46 x 25 cm, Chiral Technologies, Inc.), 25% MeOH in CO_2, 3 mL/min, 35 °C, and UV detection at 215 nm, (*R*)-**3a** {$[\alpha]_D$ = +36.9 (c = 1.18, MeOH)} was peak 1 at 3.0 min. and (*S*)-**3a** {$[\alpha]_D$ = -38.8 (c = 1.28, MeOH)} was peak 2 at 5.4 min. An analytical sample was obtained by reverse phase chromatography which gave **3a**·1TFA for characterization. MS (ESI) *m/z*: 467.0 $(M+2+H)^+$. ^{1}H NMR (500 MHz, CD_3OD) δ 7.99 (d, *J*=1.65 Hz, 1H), 7.60 (s, 1H), 7.56 (dd, *J*=1.92, 8.52 Hz, 1H), 7.44 (d, *J*=8.25 Hz, 1H), 5.81 (tdd, *J*=7.15, 10.04, 16.91 Hz, 1H), 5.12-5.20 (m, 2H), 4.91-4.96 (m, 1H), 3.77 (s, 3H), 2.64-2.78 (m, 2H), 1.44 (s, 9H). ^{13}C NMR (125 MHz, CD_3OD) δ 157.5, 156.1, 149.9, 143.5, 133.1, 133.0, 132.9, 124.2, 123.7, 122.9, 120.6, 118.8, 118.7, 81.6, 53.0, 49.6 (overlaps with CD_3OD), 38.5, 28.7.

Methyl *N*-[(14*S*)-17-chloro-14-[(2*E*)-3-[5-chloro-2-(1H-1,2,3,4-tetrazol-1- yl)phenyl]prop-2-enamido]-16,18-diazatricyclo[13.2.1.0^{2,7}]octadeca-1(17),2,4,6,15(18)-pentaen-5-yl]-carbamate, trifluoroacetic acid salt (4). To a vial containing a solution of **3** (0.012 g, 0.018 mmol) in ACN (0.30 mL)/$CHCl_3$ (0.30 mL) was added NCS (2.85 mg, 0.021 mmol). The vial was sealed with a teflon-coated screw cap and the reaction was warmed to 65 °C. After 4 h, additional NCS (2.85 mg, 0.021 mmol) was added. After another 1 h, the reaction was cooled to rt and then the reaction was concentrated. Purification by reverse phase chromatography

afforded **4** (0.0040 g, 31%) as a yellow solid. MS (ESI) *m/z*: 595.1 $(M+H)^+$. ^{1}H NMR (500 MHz, CD_3OD, 50 °C) δ ppm 9.46 (s, 1 H), 7.97 (d, *J*=2.2 Hz, 1 H), 7.65 (dd, *J*=8.8, 2.2 Hz, 1 H), 7.55 (d, *J*=8.3 Hz, 1 H), 7.40 (d, *J*=2.2 Hz, 1 H), 7.36 (dd, *J*=8.3, 1.6 Hz, 1 H), 7.27 (d, *J*=8.2 Hz, 1 H), 7.13 (d, *J*=15.4 Hz, 1 H), 6.77 (d, *J*=15.9 Hz, 1 H), 4.85 (dd, *J*=10.4, 5.5 Hz, 1 H), 3.75 (s, 3 H), 2.43 - 2.52 (m, 1 H), 2.31 - 2.40 (m, 1 H), 2.05 - 2.15 (m, 1 H), 1.57 - 1.68 (m, 1 H), 1.10 - 1.53 (m, 6 H), 0.95 - 1.07 (m, 1 H), 0.26-0.38 (m, 1 H).

***tert*-Butyl *N*-[(1*S*)-1-(4-{2-bromo-4-[(methoxycarbonyl)amino]phenyl}-1-{[2- (trimethylsilyl)ethoxy]methyl}-1H-imidazol-2-yl)but-3-en-1-yl]carbamate (4a)**. To a cooled (0 °C) suspension of NaH (0.343 g, 8.58 mmol) in THF (15 mL) was added dropwise a clear, yellow solution of **3a** (3.63 g, 7.80 mmol) in THF (15 mL). After 30 min, the reaction was allowed to warm to rt. After 2.5 h the reaction was a thick, viscous mixture so DMF (6 mL) was added to facilitate stirring. The resulting clear, dark yellow solution was cooled to 0 °C and then SEM-Cl (1.38 mL, 7.80 mmol) was added dropwise. After 30 min, additional SEM-Cl (0.20 equiv.) was added. After another 30 min the reaction was quenched with sat. NH_4Cl and the reaction was allowed to warm to rt. The reaction was extracted with EtOAc (2x). The organic layers were combined and washed with sat. $NaHCO_3$, brine, dried over Na_2SO_4, filtered, and concentrated to give a clear, thick viscous orange oil. Purification by normal phase chromatography (gradient 0-50% EtOAc/Hex) gave **4a** (2.35 g, 51%) as a white solid and **5a** (0.757 g) as a clear, colorless oil. For **4a**: MS (ESI) *m/z*: 595.1 $(M+H)^+$ and 597.2 $(M+2+H)^+$. ^{1}H NMR (500 MHz, CD_3OD) δ 7.87 (s, 1H), 7.66 (d, *J*=8.25 Hz, 1H), 7.55 (s, 1H), 7.41 (dd, *J*=2.20, 8.80 Hz, 1H), 5.75-5.86 (m, 1H), 5.62 (d, *J*=11.00 Hz, 1H), 5.33 (d, *J*=11.00 Hz, 1H), 5.14 (d, *J*=17.05 Hz, 1H), 5.05 (d, *J*=9.90 Hz, 1H), 4.96 (t, *J*=7.15 Hz, 1H), 3.75 (s, 3H), 3.60 (t, *J*=7.97 Hz, 2H), 2.60-2.74 (m,

2H), 1.43 (s, 9H), 0.87-1.02 (m, 2H), 0.00 (s, 9H). ^{13}C NMR (125 MHz, CD_3OD) δ 157.6, 156.3, 149.8, 140.6, 138.8, 135.4, 132.0, 130.3, 123.9, 122.8, 121.0, 118.7, 118.6, 80.7, 76.4, 67.4, 52.8, 47.8, 40.0, 28.9, 18.9, -1.2. For **5a**: MS (ESI) *m/z*: 725.3 $(M+H)^+$ and 727.2 $(M+2+H)^+$. ^{1}H NMR (500 MHz, CD_3OD) δ 7.81 (d, *J*=8.25 Hz, 1H), 7.68 (s, 1H), 7.64 (d, *J*=2.20 Hz, 1H), 7.35 (dd, *J*=2.20, 8.25 Hz, 1H), 5.75-5.86 (m, 1H), 5.63 (d, *J*=11.00 Hz, 1H), 5.35 (d, *J*=11.00 Hz, 1H), 5.14 (d, *J*=17.05 Hz, 1H), 5.02-5.08 (m, 3H), 4.97 (t, *J*=7.42 Hz, 1H), 3.74 (s, 3H), 3.64-3.69 (m, 2H), 3.57-3.63 (m, 2H), 2.60-2.77 (m, 2H), 1.42 (s, 9H), 0.88-1.02 (m, 4H), 0.02 (s, 9H), 0.00 (s, 9H).

***tert*-Butyl *N*-[(1*S*)-1-(4-{4-[(methoxycarbonyl)amino]-2-(pent-4-en-1-yl)phenyl}-1-{[2-(trimethylsilyl)ethoxy]methyl}-1H-imidazol-2-yl)but-3-en-1-yl]carbamate (4b).** To a flame-dried, thick-walled vial was placed **4a** (0.366 g, 0.62 mmol), pent-4-enylboronic acid (0.154 g, 1.35 mmol), Ag_2O (0.712 g, 3.07 mmol), K_2CO_3 (0.510 g, 3.69 mmol), and $PdCl_2(dppf)\cdot CH_2Cl_2$ adduct (0.050 g, 0.061 mmol). The vial was purged with argon for several minutes and then degassed THF (2.6 mL) was added. The vial was sealed with a teflon-coated screw cap and the black suspension was warmed to 80 °C. After 8 h the reaction was cooled to rt. The reaction mixture was filtered and the filtrate was concentrated to give a brown foam. Purification by normal phase chromatography (gradient elution 0-30% EtOAc/Hex) gave impure material. The impure material was purified by reverse phase chromatography. The pure fractions were combined, neutralized with sat. $NaHCO_3$, and then concentrated to give a white solid. The white solid was partitioned between water and EtOAc and the layers were separated. The aqueous layer was extracted with EtOAc (1x). The organic layers were combined and washed with brine, dried over Na_2SO_4, filtered and concentrated to afford the **4b** (0.054 g, 15%) as a white foam.

MS (ESI) *m/z*: 585.3 $(M+H)^+$. ^{1}H NMR (400 MHz, CD_3OD) δ 7.27-7.36 (m, 3H), 7.11 (s, 1H), 5.67-5.84 (m, 2H), 5.64 (d, *J*=10.99 Hz, 1H), 5.31 (d, *J*=10.99 Hz, 1H), 5.12 (d, *J*=16.26 Hz, 1H), 5.03 (d, *J*=9.67 Hz, 1H), 4.85-4.98 (m, 3H), 3.73 (s, 3H), 3.58 (t, *J*=8.13 Hz, 2H), 2.55-2.84 (m, 4H), 1.94-2.05 (m, 2H), 1.49-1.62 (m, 2H), 1.42 (s, 9H), 0.84-1.03 (m, 2H), 0.00 (s, 9H).

***tert*-Butyl *N*-[(1*S*)-1-{4-[2-bromo-4-(9,9-dimethyl-3-oxo-2,6-dioxa-4-aza-9-siladecan- 4-yl)phenyl]-1-{[2-(trimethylsilyl)ethoxy]methyl}-1H-imidazol-2-yl}but-3-en-1- yl]carbamate (5a).** Compound **5a** was prepared as a by-product in the preparation of compound **4a**. Please see experimental procedure for compound **4a** for preparation and characterization of **5a**.

***tert*-Butyl *N*-[(1*S*)-1-(4-{2-amino-4-[(methoxycarbonyl)amino]phenyl}-1-{[2- (trimethyl-silyl)ethoxy]methyl}-1H-imidazol-2-yl)but-3-en-1-yl]carbamate (6a)**. A thick-walled vial containing **4a** (2.0 g, 3.36 mmol), CuI (0.128 g, 0.67 mmol), L-proline (0.155 g, 1.34 mmol) and K_2CO_3 (1.39 g, 10.1 mmol) in DMSO (6.7 mL) was vacuumed and back-filled with argon three times. Then 28% aq. NH_4OH (0.61 mL, 4.37 mmol) was added. The vial was sealed with a teflon-coated screw cap and the reaction was warmed to 85 °C. After 20 h, the reaction was cooled to rt, diluted with EtOAc, washed with water, brine, dried over Na_2SO_4, filtered and concentrated. Purification by normal phase chromatography (gradient elution 0-40% EtOAc/Hex) afforded **6a** (1.05 g, 59%) as a yellow solid. MS (ESI) *m/z*: 532.5 $(M+H)^+$. ^{1}H NMR (500 MHz, CD_3OD) δ 7.29 (s, 1H), 7.27 (d, *J*=8.53 Hz, 1H), 6.95-6.98 (m, 1H), 6.73 (dd, *J*=2.06, 8.39 Hz, 1H), 5.75-5.86 (m, 1H), 5.57 (d, *J*=11.00 Hz, 1H), 5.30 (d, *J*=11.00 Hz, 1H), 5.13 (d, *J*=16.23 Hz, 1H), 5.04 (d, *J*=10.18 Hz, 1H), 4.92-4.97 (m, 1H), 3.72 (s, 3H), 3.58 (t, *J*=8.12 Hz, 2H), 2.68-2.76 (m, 1H), 2.60-2.68 (m, 1H), 1.42 (s, 9H), 0.87-0.99 (m, 2H), 0.00 (s,

9H). ^{13}C NMR (100 MHz, $CDCl_3$) δ 155.1, 153.9, 146.9, 145.6, 140.5, 137.7, 133.6, 127.7, 118.3, 115.1, 113.0, 108.0,106.0, 79.7, 74.9, 66.3, 52.2, 46.1, 39.4, 28.4, 17.8, -1.4.

***tert*-Butyl *N*-[(1*S*)-1-(4-{4-[(methoxycarbonyl)amino]-2-(pent-4-enamido)phenyl}- 1-{[2-(trimethylsilyl)ethoxy]methyl}-1H-imidazol-2-yl)but-3-en-1-yl]carbamate (7a)**. To a cooled (-10 °C) solution of **6a** (1.34 g, 2.52 mmol), pent-4-enoic acid (0.26 mL, 2.52 mmol) and Hunig's base (1.32 mL, 7.56 mmol) in EtOAc (72 mL) was added a solution of 50% 1-propanephosphonic acid cyclic anhydride in EtOAc (2.97 mL, 5.04 mmol). Following the addition, the reaction was allowed to warm to rt. After 2 h, the reaction was concentrated and purified by normal phase chromatography (gradient elution 0-40% EtOAc/Hex) which gave **7a** (1.33 g, 86%) as a yellow solid. MS (ESI) *m/z*: 614.2 $(M+H)^+$. ^{1}H NMR (400 MHz, CD_3OD) δ 8.43 (d, *J*=2.20 Hz, 1H), 7.50-7.57 (m, 2H), 7.33 (d, *J*=7.70 Hz, 1H), 7.13 (d, *J*=8.24 Hz, 1H, NH), 5.76-5.98 (m, 2H), 5.60 (d, *J*=10.44 Hz, 1H), 5.34 (d, *J*=10.99 Hz, 1H), 4.92-5.20 (m, 5H), 3.73 (s, 3H), 3.60 (t, *J*=8.25 Hz, 2H), 2.66-2.85 (m, 2H), 2.54-2.62 (m, 2H), 2.44-2.54 (m, 2H), 1.43 (s, 9H), 0.87-1.02 (m, 2H), 0.00 (s, 9H). ^{13}C NMR (100 MHz, CD_3OD) δ 173.5, 157.8, 156.7, 149.0, 140.4, 139.6, 138.4, 137.5, 135.5, 128.0, 118.7, 118.5, 117.8, 116.3, 115.5, 112.5, 80.7, 76.4, 67.5, 52.7, 47.9, 39.8, 38.9, 31.2, 29.0, 18.9, -1.1.

***tert*-Butyl *N*-[(11*E*,14*S*)-5-[(methoxycarbonyl)amino]-16-{[2-(trimethylsilyl)ethoxy]-methyl}-16,18-diazatricyclo[13.2.1.0^{2,7}]octadeca-1(17),2,4,6,11,15(18)-hexaen-14-yl]carbamate (8a) and *tert*-Butyl *N*-[(11*Z*,14*S*)-5-[(methoxycarbonyl)amino]-16-{[2-(trimethylsilyl)ethoxy]-methyl}-16,18-diazatricyclo[13.2.1.0^{2,7}]octadeca-1(17),2,4,6,11,15(18)-hexaen-14-yl]-carbamate (8b).** (Flask 1): To a flame-dried flask was added Grubbs (II) (0.087 g, 0.10 mmol).

The flask was degassed with argon for several minutes and then degassed DCM (3 mL) was added to give a clear, burgundy solution. (Flask 2): To a separate flame-dried RBF was added **4b** (0.150 g, 0.26 mmol), p-toluenesulfonic acid monohydrate (0.054 g, 0.28 mmol) and DCM (366 mL). The flask was equipped with a reflux condenser and the solution was degassed with argon for 30 min. The reaction was heated to 40 °C. After 1 h, the solution of Grubbs (II) from flask one was added dropwise to flask 2. After 1.5 h, the reaction was cooled to rt, washed with sat. $NaHCO_3$, brine, dried over $MgSO_4$, filtered and concentrated to give a brown foam. HPLC of the reaction mixture prior to purification indicated a 3.2:1 *E*:*Z* alkene ratio. The E/Z-alkene isomers were separated by reverse phase chromatography. The pure fractions of each isomer were combined, neutralized with sat. $NaHCO_3$, and then concentrated to give a white solid. The white solid was partitioned between water and EtOAc and the layers were separated. The aqueous layer was extracted with EtOAc (1x). The organic layers were combined and washed with brine, dried over Na_2SO_4, filtered and concentrated to afford *E*-alkene **8a** (0.058 g, 41%, peak 1) as a clear, pale brown oil and *Z*-alkene **8b** (0.016 g, 11%, peak 2) as a clear, pale brown oil. For *E*-alkene **8a**: MS (ESI) *m/z*: 557.4 $(M+H)^+$. ^{1}H NMR (500 MHz, $CDCl_3$, 50 °C) δ 7.20-7.25 (m, 3H), 6.85 (s, 1H), 6.60 (s, 1H), 5.97-6.08 (m, 1H), 5.49 (ddd, *J*=4.95, 10.17, 15.12 Hz, 1H), 5.38 (d, *J*=11.00 Hz, 1H), 5.19-5.27 (m, 1H), 5.16 (d, *J*=10.45 Hz, 1H), 4.64-4.77 (m, 1H), 3.79 (s, 3H), 3.54-3.72 (m, 3H), 2.72-2.82 (m, 1H), 2.23-2.36 (m, 2H), 1.91-2.01 (m, 1H), 1.66-1.80 (m, 2H), 1.46 (s, 9H), 0.83-1.06 (m, 3H), 0.02 (s, 9H). ^{1}H-^{1}H-homonuclear decoupling of the two sets of vicinal methylene protons which revealed the *J* coupling constant between the double bond protons *J* = 14.8-15.4 Hz. ^{13}C NMR (125 MHz, CD_3OD) δ 157.4, 156.6, 148.1, 145.0, 139.9, 139.7, 136.4, 130.7, 129.1, 126.8, 121.5, 119.9, 117.0, 80.8, 76.1, 67.5, 52.6, 50.9, 39.7, 32.6, 32.1, 32.0, 28.9, 18.9, -1.2. For *Z*-alkene **8b**: MS (ESI) *m/z*: 557.3 $(M+H)^+$.

Methyl *N*-[(15*S*)-18-chloro-15-[(2*E*)-3-[5-chloro-2-(1H-1,2,3,4-tetrazol-1-yl)phenyl]-prop-2-enamido]-17,19-diazatricyclo[14.2.1.0^{2,7}]nonadeca-1(18),2,4,6,16(19)-pentaen-5-yl]-carbamate, trifluoroacetic acid salt (9). Using a procedure analogous to that which was used to prepare **4**, **8** was converted to **9** (0.0060 g, 33%) as a white solid. MS (ESI) *m/z*: 609.1 $(M+H)^+$. ^{1}H NMR (500 MHz, CD_3OD, 50 °C) δ ppm 9.45 (s, 1 H), 7.95 (d, *J*=2.2 Hz, 1 H), 7.64 (dd, *J*=8.8, 2.2 Hz, 1 H), 7.55 (d, *J*=8.2 Hz, 1 H), 7.40 (d, *J*=2.2 Hz, 1 H), 7.35 (dd, *J*=8.2, 2.2 Hz, 1 H), 7.25 (d, *J*=8.2 Hz, 1 H), 7.13 (d, *J*=15.4 Hz, 1 H), 6.75 (d, *J*=15.9 Hz, 1 H), 4.90 (dd, *J*=9.9, 4.4 Hz, 1 H), 3.75 (s, 3 H), 2.62 - 2.73 (m, 1 H), 2.35 - 2.45 (m, 1 H), 2.07 - 2.16 (m, 1 H), 1.89 - 1.99 (m, 1 H), 1.56 - 1.67 (m, 1 H), 1.22 - 1.45 (m, 7 H), 0.72 - 0.86 (m, 1 H), 0.47-0.58 (d, 1 H).

Methyl *N*-[(11*E*,14*S*)-14-amino-16,18-diazatricyclo[13.2.1.0^{2,7}]octadeca-1(17),2,4,6,11,15-(18)-hexaen-5-yl]carbamate (9a). A clear, colorless solution of **8a** (0.024 g, 0.043 mmol) in MeOH (0.86 mL) and 5 M HCl (aq) (0.34 mL, 1.72 mmol) was warmed to 50 °C. After 1.5 h, additional 5 M HCl (aq) (0.34 mL, 1.72 mmol) was added and the reaction was warmed to 75 °C. After 2 h, additional 5 M HCl (aq) (0.34 mL, 1.72 mmol) was added and the reaction was heated at 75 °C. After 3 h, the reaction was stopped, cooled to 0 °C, neutralized with 6 M NaOH and then the reaction was concentrated to give **9a**. The product was used in the next step without further purification. MS (ESI) *m/z*: 327.1 $(M+H)^+$.

Methyl *N*-[(14*S*)-14-amino-16,18-diazatricyclo[13.2.1.0^{2,7}]octadeca- 1(17),2,4,6,15(18)-pentaen-5-yl]carbamate, *bis*-trifluoroacetic acid salt (9b). To a mixture of **8a** and **8b** (0.074 g, 0.13 mmol) in MeOH (2 mL) was added 10% palladium on carbon (0.014 g, 0.013 mmol). The reaction mixture was stirred under an atmosphere of hydrogen (balloon). After 2 h, the reaction

was filtered through a 0.45 μm glass microfiber filter and rinsed with MeOH. The filtrate was concentrated to give *tert*-butyl *N*-[(14*S*)-5-[(methoxycarbonyl)amino]- 16-{[2-(trimethylsilyl)ethoxy]methyl}-16,18-diazatricyclo[13.2.1.$0^{2,7}$]octadeca-1(17),2,4,6,15(18)-pentaen-14-yl]carbamate (0.062 g, 83%) as a white solid which was used in the next step without further purification. MS (ESI) *m/z*: 559.6 $(M+H)^+$.

A clear, colorless solution of *tert*-butyl *N*-[(14*S*)-5-[(methoxycarbonyl)amino]- 16-{[2-(trimethylsilyl)ethoxy]methyl}-16,18-diazatricyclo[13.2.1.$0^{2,7}$]octadeca-1(17),2,4,6,15(18)-pentaen-14-yl]carbamate (0.062 g, 0.11 mmol) in MeOH (0.50 mL) and 5 M HCl (aq) (0.5 mL, 2.50 mmol) warmed to 75 °C. After 4 h, the reaction was cooled to rt and concentrated. Purification by reverse phase chromatography gave **9b** (0.058 g, 94%) as a white solid. MS (ESI) *m/z*: 329.4 $(M+H)^+$. ^{1}H NMR (400 MHz, CD_3OD) δ 7.58 (s, 1H), 7.43 - 7.50 (m, 2H), 7.36 - 7.40 (m, 1H), 4.77 (dd, *J*=11.0, 5.5 Hz, 1H), 3.75 (s, 3H), 2.58 - 2.70 (m, 1H), 2.29 - 2.48 (m, 2H), 1.84 - 1.96 (m, 1H), 1.07 - 1.50 (m, 7H), 0.32 - 0.54 (m, 1H).

Methyl *N*-[(15*S*)-15-[(2*E*)-3-[5-chloro-2-(1H-1,2,3,4-tetrazol-1-yl)phenyl]prop-2- enamido]-8-oxa-17,19-diazatricyclo[14.2.1.$0^{2,7}$]nonadeca-1(18),2,4,6,16(19)-pentaen-5-yl]carbamate, trifluoroacetic acid salt (11). Using a procedure analogous to that which was used to prepare **2**, **9g** (0.093 g, 0.16 mmol) was coupled to **10a** to give **11** (0.102 g, 91%) as a white solid. MS (ESI) *m/z*: 577.2 $(M+H)^+$. ^{1}H NMR (500 MHz, CD_3OD) δ ppm 9.52 (s, 1 H), 7.97 (d, *J*=2.2 Hz, 1 H), 7.67 (dd, *J*=8.8, 2.2 Hz, 1 H), 7.58 (d, *J*=8.8 Hz, 1 H), 7.40 (s, 1 H), 7.33 - 7.38 (m, 2 H), 7.14 (d, *J*=15.4 Hz, 1 H), 7.06 (d, *J*=8.2 Hz, 1 H), 6.78 (d, *J*=15.9 Hz, 1 H), 5.04 (dd, *J*=9.9, 4.4 Hz, 1 H), 4.05 - 4.10 (m, 1 H), 3.93 (td, *J*=8.2, 2.7 Hz, 1 H), 3.75 (s, 3 H), 2.19 - 2.27 (m, 1 H), 1.94 - 2.03 (m, 1 H), 1.69 - 1.83 (m, 2 H), 1.49 - 1.63 (m, 4 H), 0.91 - 1.09 (m, 2 H).

tert-Butyl _N_-[(12_E_,15_S_)-5-[(methoxycarbonyl)amino]-9-oxo-17-{[2-(trimethylsilyl)-ethoxy]-methyl}-8,17,19-triazatricyclo[14.2.1.0^{2,7}]nonadeca-1(18),2,4,6,12,16(19)- hexaen-15-yl]-carbamate (11a) and _tert_-Butyl _N_-[(12_Z_,15_S_)-5-[(methoxycarbonyl)-amino]-9-oxo-17-{[2-(trimethylsilyl)ethoxy]methyl}8,17,19-triazatricyclo-[14.2.1.0^{2,7}]nonadeca-1(18),2,4,6,12,16-(19)-hexaen-15-yl]carbamate (11b). (Flask 1): To a flame-dried flask was added Grubbs (II) (0.394 g, 0.46 mmol). The flask was degassed with argon for several minutes and then degassed DCM (2 mL) was added to give a clear, burgundy solution. (Flask 2): To a separate flame-dried RBF was added **7a** (5.7 g, 9.29 mmol), p-toluenesulfonic acid monohydrate (1.94 g, 10.21 mmol) and DCM (774 mL). The flask was equipped with a reflux condenser and the solution was degassed with argon for 30 min. The reaction was heated to 40 °C. After 1 h, the solution of Grubbs (II) from flask one was added dropwise to flask 2. After 1.5 h, the reaction was cooled to rt and the reaction was washed with sat. $NaHCO_3$, brine, dried over $MgSO_4$, filtered and concentrated to give a brown solid. HPLC of the reaction mixture prior to purification indicated a 1.6:1 *E*:*Z* alkene ratio. Purification by normal phase chromatography (gradient elution 0-20% MeOH/DCM) gave a 1.7:1 *E*-alkene **11a**:*Z*-alkene **11b** (4.75 g, 87%) as a yellow solid. The *E*/*Z*-alkene isomers were separated by reverse phase chromatography. The pure fractions of each isomer were combined, neutralized with sat. $NaHCO_3$, and then concentrated to give a white solid. The white solid was partitioned between water and EtOAc and the layers were separated. The aqueous layer was extracted with EtOAc (1x). The organic layers were combined and washed with brine, dried over Na_2SO_4, filtered and concentrated to afford *E*-alkene **11a** (2.41 g, 44%, peak 1) as an off-white solid and the *Z*-alkene **11b** (1.75 g, 32%, peak 2) as an off-white solid. For *E*-alkene **11a**: Note that the following characterization was done on

the TFA salt. MS (ESI) *m/z*: 586.2 $(M+H)^+$. ^{1}H NMR (400 MHz, CD_3OD) δ 7.57 (s, 2H), 7.36 - 7.47 (m, 2H), 5.77 (d, *J*=11.0 Hz, 1H), 5.60 (d, *J*=11.0 Hz, 1H), 5.35 - 5.56 (m, 2H), 5.13 (t, *J*=6.0 Hz, 1H), 3.67 - 3.83 (m, 5H), 2.63 - 2.77 (m, 2H), 2.23 - 2.56 (m, 4H), 1.41 (s, 9H), 0.95 - 1.13 (m, 2H), 0.07 (s, 9H). The *E*-alkene geometry was determined on compound **12c**. ^{13}C NMR (100 MHz, CD_3OD) δ 173.7, 157.8, 156.2, 148.3, 143.4, 138.2, 136.1, 132.5, 132.1, 126.0, 120.8, 119.3, 117.6, 81.6, 78.4, 69.0, 52.9, 36.5, 36.4, 28.9, 28.7, 19.0, -1.2. Note: one carbon overlaps with CD_3OD. $[\alpha]_D$ = 24.1 (c = 1.43, MeOH). For *Z*-alkene **11b**: Note that the following characterization was done on the TFA salt. MS (ESI) *m/z*: 586.5 $(M+H)^+$. ^{1}H NMR (400 MHz, CD_3OD) δ 9.57 (s, 1H, NH), 7.64 (s, 1H), 7.53 (s, 1H), 7.40 (d, *J*=8.25 Hz, 1H), 7.35-7.39 (m, 1H), 6.01 (d, *J*=10.44 Hz, 1H), 5.30-5.55 (m, 3H), 5.14 (dd, *J*=4.67, 11.27 Hz, 1H), 3.75 (s, 3H), 3.58-3.74 (m, 2H), 2.91-3.10 (m, 1H), 2.53-2.80 (m, 3H), 2.22-2.34 (m, 1H), 2.09-2.22 (m, 1H), 1.39 (s, 9H), 1.01-1.11 (m, 1H), 0.91-1.00 (m, 1H), 0.05 (s, 9H). ^{13}C NMR (100 MHz, CD_3OD) δ 173.2, 157.7, 156.2, 148.4, 143.0, 137.9, 134.6, 134.0, 132.1, 124.2, 119.5, 118.8, 117.5, 116.2, 81.5, 78.7, 68.8, 52.8, 47.0, 38.0, 28.7, 26.0, 19.0, -1.2. Note: one carbon overlaps with CD_3OD.

Methyl N-[(15S)-18-chloro-15-[(2E)-3-[5-chloro-2-(1H-1,2,3,4-tetrazol-1-yl)phenyl]-prop-2-enamido]-8-oxa-17,19-diazatricyclo[14.2.1.0^{2,7}]nonadeca-1(18),2,4,6,16(19)- pentaen-5-yl]-carbamate, trifluoroacetic acid salt (12). To a solution of **11** (0.034 g, 0.049 mmol) in ACN (2.0 mL)/$CHCl_3$ (2.0 mL) was added Hunig's base (0.017 mL, 0.098 mmol). The reaction was stirred for 10 min, then NCS (7.88 mg, 0.059 mmol) was added. The reaction was capped and warmed to 65 °C. Additional NCS (39.4 mg, 0.30 mmol) was added in portions over the course of 20 h to improve conversion. The reaction was cooled to rt and concentrated. Purification by

reverse phase chromatography gave **12** (0.021 g, 59%) as a yellow solid. MS (ESI) *m/z*: 610.9 $(M+H)^+$. ^{1}H NMR (500 MHz, CD_3OD) δ ppm 9.46 (s, 1 H), 7.94 (d, *J*=2.2 Hz, 1 H), 7.64 (dd, *J*=8.3, 2.2 Hz, 1 H), 7.55 (d, *J*=8.8 Hz, 1 H), 7.32 - 7.37 (m, 2 H), 7.15 (d, *J*=15.9 Hz, 1 H), 7.05 (d, *J*=8.2 Hz, 1 H), 6.74 (d, *J*=15.4 Hz, 1 H), 4.94 (dd, *J*=9.6, 3.6 Hz, 1 H), 4.00 - 4.06 (m, 1 H), 3.88 - 3.94 (m, 1 H), 3.76 (s, 3 H), 2.12 - 2.20 (m, 1 H), 1.75 - 1.93 (m, 2 H), 1.65 - 1.74 (m, 1 H), 1.46 - 1.60 (m, 4 H), 1.0 -1.12 (m, 1 H), 0.92 - 1.02 (m, 1 H).

Methyl *N*-[(15*S*)-15-amino-9-oxo-8,17,19-triazatricyclo[14.2.1.0^{2,7}]nonadeca-1(18),2,4,6,-16(19)-pentaen-5-yl]carbamate, *bis*-trifluoroacetic acid salt (12a). Using a procedure analogous to that which was used to prepare **9b**, a mixture of **11a** and **11b** (0.054 g, 0.092 mmol) was hydrogenated and then deprotected to give **12a** (0.017 g, 32% over two steps) as a white solid. MS (ESI) *m/z*: 358.1 $(M+H)^+$. ^{1}H NMR (400 MHz, CD_3OD) δ 7.67 (s, 1H), 7.38 - 7.48 (m, 3H), 4.63 (dd, *J*=10.4, 3.8 Hz, 1H), 3.75 (s, 3H), 2.55 (ddd, *J*=14.2, 8.1, 3.0 Hz, 1H), 2.28 - 2.40 (m, 1H), 2.15 - 2.24 (m, 1H), 2.03 - 2.12 (m, 1H), 1.42 - 1.88 (m, 4H), 0.96 - 1.09 (m, 1H), 0.66 - 0.80 (m, 1H).

Methyl *N*-[(12*Z*,15*S*)-15-amino-9-oxo-8,17,19-triazatricyclo[14.2.1.0^{2,7}]nonadeca-1(18),2,4,-6,12,16(19)-hexaen-5-yl]carbamate, 2HCl (12b). A sealed tube containing a mixture of **11b** (0.030 g, 0.043 mmol) and 4M HCl in dioxane (0.50 mL, 2.0 mmol) was heated at 75 °C for 2 h. The reaction was cooled to rt and the solid was collected by filtration, rinsed with Hex, and dried to give **12b** (0.018 g, 98%) as a brown solid. MS (ESI) *m/z*: 356.2 $(M+H)^+$. ^{1}H NMR (400 MHz, CD_3OD) δ 7.48-7.56 (m, 2H), 7.37-7.44 (m, 2H), 5.49-5.62 (m, 1H), 5.19-5.32 (m, 1H), 4.79-5.03 (m, 1H), 3.72 (s, 3H), 3.41-3.58 (m, 1H), 2.82-2.98 (m, 1H), 2.63-2.79 (m, 2H), 2.10-2.32

(m, 2H). The methine proton at 4.79-5.03 ppm overlaps with the water peak and was determined by COSY experiment.

Methyl *N*-[(12*E*,15*S*)-15-amino-9-oxo-8,17,19-triazatricyclo[14.2.1.0^{2,7}]nonadeca- 1(18),2,4,-6,12,16(19)-hexaen-5-yl]carbamate, 2HCl (12c). Using a procedure analogous to that which was used to prepare **12b**, **11a** (0.612 g, 1.04 mmol) was deprotected to give **12c** (0.437 g, 98%) as a tan foam. An analytical sample was obtained by purification by reverse phase chromatography which gave **12c**·2TFA. MS (ESI) *m/z*: 356.0 $(M+H)^+$. ^{1}H NMR (500 MHz, CD_3OD) δ 7.63 (s, 1H), 7.55 (d, *J*=1.65 Hz, 1H), 7.46 (dd, *J*=1.93, 8.25 Hz, 1H), 7.43 (d, *J*=8.25 Hz, 1H), 5.52-5.59 (m, 1H), 5.40-5.48 (m, 1H), 4.93 (dd, *J*=5.23, 10.45 Hz, 1H), 3.76 (s, 3H), 2.90-2.96 (m, 1H), 2.80-2.89 (m, 1H), 2.47-2.51 (m, 2H), 2.29-2.39 (m, 2H). ^{1}H-^{1}H-homonuclear decoupling of the vicinal methylene protons revealed the *J* coupling constant between the double bond protons *J* = 15.4 Hz.

Methyl *N*-[(15*S*)-15-[(2*E*)-3-[5-chloro-2-(1H-1,2,3,4-tetrazol-1-yl)phenyl]prop-2- enamido]-9-oxo-8,17,19-triazatricyclo[14.2.1.0^{2,7}]nonadeca-1(18),2,4,6,16(19)-pentaen-5-yl]carbamate, trifluoroacetic acid salt (13). Using a procedure analogous to that which was used to prepare **2**, **12a** (0.030 g, 0.051 mmol) was coupled to **10a** to give **13** (0.020 g, 54%) as a white solid. MS (ESI) *m/z*: 590.1 $(M+H)^+$. ^{1}H NMR (400 MHz, CD_3OD) δ ppm 9.50 (s, 1 H), 7.96 (d, *J*=2.2 Hz, 1 H), 7.67 (dd, *J*=8.8, 2.2 Hz, 1 H), 7.61 (s, 1 H), 7.57 (d, *J*=8.2 Hz, 1 H), 7.38 - 7.45 (m, 3 H), 7.12 (d, *J*=15.9 Hz, 1 H), 6.74 (d, *J*=15.9 Hz, 1 H), 5.01 (dd, *J*=10.2, 4.7 Hz, 1 H), 3.75 (s, 3 H), 2.28 - 2.41 (m, 2 H), 2.15 - 2.25 (m, 1 H), 1.95 - 2.07 (m, 1 H), 1.41 - 1.76 (m, 4 H), 0.71 - 0.98 (m, 2 H).

tert-Butyl _N_-[(11_E_,14_S_)-5-[(methoxycarbonyl)amino]-9-oxo-16-{[2-(trimethylsilyl)-ethoxy]-methyl}-8,16,18-triazatricyclo[13.2.1.0^{2,7}]octadeca-1(17),2,4,6,11,15(18)- hexaen-14-yl]-carbamate and _tert_-Butyl _N_-[(11_Z_,14_S_)-5-[(methoxycarbonyl)-amino]-9-oxo-16-{[2-(tri-methylsilyl)ethoxy]methyl}-8,16,18-triazatricyclo[13.2.1.0^{2,7}]octadeca-1(17),2,4,6,11,15(18)-hexaen-14-yl]carbamate (13a). Using a procedure analogous to that which was used to prepare **8a** and **8b**, **7b** (0.400 g, 0.68 mmol) was subjected to ring-closing metathesis and the reaction was purified by normal phase chromatography (0-4% MeOH/DCM) which gave **13a** (0.250 g, 66 %) as a 2.2:1 mixture of *E*-alkene:*Z*-alkene isomers and as a yellow solid. Note that the Z-alkene isomer is the first eluting (peak 1) isomer on the analytical reverse phase HPLC. MS (ESI) *m/z*: 572.2 $(M+H)^+$.

Methyl _N_-[(14_S_)-14-amino-9-oxo-8,16,18-triazatricyclo[13.2.1.0^{2,7}]octadeca- 1(17),2,4,6,15-(18)-pentaen-5-yl]carbamate, 2HCl salt (14a). To a suspension of **13a** (0.25 g, 0.44 mmol) in MeOH (10 mL) and EtOAc (5 mL) was added 10% palladium on carbon (0.047 g, 0.044 mmol). Hydrogen gas was bubbled through the reaction mixture for 5 min and then the reaction was stirred vigorously under a hydrogen atmosphere (balloon). After 24 h, the reaction was filtered through a 0.45 μm glass microfiber filter, rinsing with MeOH, DCM and EtOAc. The filtrate was concentrated and purification by reverse phase chromatography afforded *tert*-butyl *N*-[(14*S*)-5-[(methoxycarbonyl)amino]-9-oxo-16-{[2-(trimethylsilyl)ethoxy]methyl}-8,16,18-triazatricyclo[13.2.1.0^{2,7}]-octadeca-1(17),2,4,6,15(18)-pentaen-14-yl]carbamate (0.220 g, 88%) as an off-white solid. MS (ESI) *m/z*: 574.4 $(M+H)^+$. ^{1}H NMR (500 MHz, CD_3OD, 60 °C) δ 7.76 (d, *J*=2.20 Hz, 1H), 7.47 (d, *J*=8.53 Hz, 1H), 7.36 (dd, *J*=2.20, 8.53 Hz, 1H), 7.27 (s, 1H), 5.48

(d, *J*=10.73 Hz, 1H), 5.33 (d, *J*=10.73 Hz, 1H), 4.96 (dd, *J*=4.68, 9.63 Hz, 1H), 3.74 (s, 3H), 3.60 (t, *J*=8.12 Hz, 2H), 2.46-2.55 (m, 1H), 2.34-2.41 (m, 1H), 2.11-2.21 (m, 1H), 1.87-1.99 (m, 2H), 1.71-1.82 (m, 1H), 1.46 (s, 10H), 1.08-1.19 (m, 1H), 0.91-0.96 (m, 2H), 0.00 (s, 9H). ^{13}C NMR (101 MHz, $CDCl_3$) δ 171.4, 154.9, 154.1, 145.7, 138.6, 138.0, 136.6, 126.4, 117.5, 117.1, 113.8, 112.6, 80.1, 75.1, 66.6, 52.1, 46.9, 37.0, 34.1, 28.3, 24.94, 24.86, 17.8, -1.4.

A sealed vial containing a mixture of *tert*-butyl *N*-[(14*S*)- 5-[(methoxy-carbonyl)amino]-9-oxo-16-{[2-(trimethylsilyl)ethoxy]methyl}-8,16,18-triazatricyclo-[13.2.1.0^{2,7}]-octadeca-1(17),2,4,6,15(18)-pentaen-14-yl]carbamate (0.099 g, 0.173 mmol) and 4M HCl in dioxane (2 mL, 8.00 mmol) was heated at 50 °C. After 2 h, the yellow suspension was cooled to rt and then concentrated. The residue was suspended in MeOH and Et_2O. The solid was collected by filtration. The solid was rinsed with Et_2O, air-dried (very hygroscopic) to afford **14a** (0.053 g, 74%) as a yellow solid. MS (ESI) *m/z*: 344.2 $(M+H)^+$. ^{1}H NMR (400 MHz, CD_3OD) δ 7.65 (s, 1H), 7.40-7.53 (m, 3H), 3.72 (s, 3H), 3.22-3.28 (m, 1H), 2.47-2.57 (m, 1H), 2.13-2.40 (m, 3H), 1.66-1.82 (m, 1H), 1.49-1.64 (m, 1H), 0.91-1.21 (m, 2H). ^{13}C NMR (101 MHz, CD_3OD) δ 173.5, 156.2, 143.6, 142.0, 137.6, 133.6, 131.2, 119.2, 118.6, 118.2, 118.0, 53.0, 47.9, 35.3, 32.0, 23.7, 22.4.

Methyl *N*-[(12*E*,15*S*)-15-[(2*E*)-3-[5-chloro-2-(1H-1,2,3,4-tetrazol-1-yl)phenyl]prop- 2-enamido]-9-oxo-8,17,19-triazatricyclo[14.2.1.0^{2,7}]nonadeca-1(18),2,4,6,12,16(19)- hexaen-5-yl]carbamate, trifluoroacetic acid salt (16). Using a procedure analogous to that which was used to prepare **2**, **12c** (0.080 g, 0.19 mmol) was coupled to **10a** to give **16** (0.037 g, 28%) as an off-white solid. MS (ESI) *m/z*: 588.1 $(M+H)^+$. ^{1}H NMR (500 MHz, CD_3OD) δ ppm 9.51 (s, 1 H), 7.97 (d, *J*=2.2 Hz, 1 H), 7.68 (dd, *J*=8.5, 2.5 Hz, 1 H), 7.58 (d, *J*=8.2 Hz, 2 H), 7.37 - 7.41

(m, 3 H), 7.14 (d, *J*=15.4 Hz, 1 H), 6.76 (d, *J*=15.4 Hz, 1 H), 5.50 - 5.59 (m, 1 H), 5.37 - 5.45 (m, 1 H), 5.08 (dd, *J*=10.2, 4.7 Hz, 1 H), 3.75 (s, 3 H), 2.76 - 2.84 (m, 1 H), 2.32 - 2.60 (m, 5 H). ^{13}C NMR (125 MHz, CD_3OD) δ 174.3, 167.4, 156.2, 148.1, 146.0, 143.3, 138.5, 138.1, 136.3, 135.0, 134.3, 132.8, 132.6, 132.2, 132.1, 129.7, 128.8, 126.5, 126.1, 120.0, 118.0, 117.9, 117.5, 52.9, 49.2 (overlaps with CD_3OD), 37.5, 36.4, 28.9.

Methyl *N*-[(12*E*,15*S*)-18-chloro-15-[(2*E*)-3-[5-chloro-2-(1H-1,2,3,4-tetrazol-1- yl)-phenyl]prop-2-enamido]-9-oxo-8,17,19-triazatricyclo[14.2.1.0^{2,7}]nonadeca-1(18),2,4,-6,12,16(19)-hexaen-5-yl]carbamate, trifluoroacetic acid salt (17). Using a procedure analogous to that which was used to prepare **4**, **16** (0.0481 g, 0.082 mmol) was converted to **17** (0.028 g, 44%) as a white solid. MS (ESI) *m/z*: 622.0 $(M+H)^+$. ^{1}H NMR (400 MHz, DMSO-d_6 +2 drops D_2O) δ ppm 9.76 (s, 1 H), 7.92 (d, *J*=2.2 Hz, 1 H), 7.68 (dd, *J*=8.2, 2.2 Hz, 1 H), 7.64 (d, *J*=8.2 Hz, 1 H), 7.38 (s, 1 H), 7.31 (dd, *J*=8.8, 2.2 Hz, 1 H), 7.26 (d, *J*=8.3 Hz, 1 H), 6.77 - 6.87 (m, 2 H), 5.37 - 5.47 (m, 1 H), 5.12 - 5.21 (m, 1 H), 4.87 (dd, *J*=10.2, 4.1 Hz, 1 H), 3.61 (s, 3 H), 2.12 - 2.33 (m, 6 H).

Methyl *N*-[(14*S*)-14-[(2*E*)-3-[5-chloro-2-(1H-1,2,3,4-tetrazol-1-yl)phenyl]prop-2- enamido]-9-oxo-8,16,18-triazatricyclo[13.2.1.0^{2,7}]octadeca-1(17),2,4,6,15(18)-pentaen-5-yl]carbamate, trifluoroacetic acid salt (22). Using a procedure analogous to that which was used to prepare **2**, **14a** (0.020 g, 0.035 mmol) was coupled to **10a** to give **22** (0.012 g, 50%) as an off-white solid. MS (ESI) *m/z*: 576.0 $(M+H)^+$. ^{1}H NMR (400 MHz, CD_3OD) δ ppm 9.51 (s, 1 H), 7.97 (d, *J*=2.2 Hz, 1 H), 7.67 (dd, *J*=8.2, 2.2 Hz, 1 H), 7.55 - 7.60 (m, 2 H), 7.50 (d, *J*=8.2 Hz, 1 H), 7.44 (s, 1 H), 7.42 (dd, *J*=8.3, 2.2 Hz, 1 H), 7.13 (d, *J*=15.4 Hz, 1 H), 6.76 (d, *J*=15.9 Hz, 1 H), 5.13 (dd,

J=10.2, 6.3 Hz, 1 H), 3.75 (s, 3 H), 2.42 - 2.52 (m, 1 H), 2.17 - 2.29 (m, 1 H), 2.05 - 2.15 (m, 1 H), 1.96 (m, 1 H), 1.51 - 1.71 (m, 2 H), 1.36 - 1.49 (m, 1 H), 0.92 - 1.07 (m, 1 H).

X-ray crystal structure data collection and structure refinement (see Supporting Information Tabulated Data). Protein for Factor XIa crystals in complex with inhibitors **9**, **13** and **16** was prepared as previously described.[20] Data for the inhibitor complex with **9** were collected at the Advanced Photon Source (APS) beamline 17-ID by Richard Walter and Gina Ranieri of Shamrock Structures. Data for complexes with inhibitors **13** and **16** were collected in the laboratory. Raw data were processed with the program HKL2000.[43] The atomic coordinates of human Factor XIa (PDB ID 4NA8) were used as a search model for rigid body only refinement in AmoRe.[44-46] Original refinement for compounds was carried out with BUSTER/TNT[47] (Global Phasing, Ltd.), MakeTNT (Global Phasing, Ltd., Cambridge, UK) for inhibitor restraint dictionaries, and COOT[48] for modeling. Later, the structures were further refined using GRADE for inhibitor restraint dictionaries. The PDB deposition numbers for compounds **9**, **13** and **16** complexed to FXIa are 5TKS, 5TKT, and 5TKU, respectively.

Enzyme Affinity Assays. Factors IXa, Xa, XIa, and activated protein C (aPC) were purchased from Haematologic Technologies. Factor XIIa, plasmin and recombinant single chain tissue-type plasminogen activator (tPA) were purchased from American Diagnostica. Plasma kallikrein and α-thrombin were purchased from Enzyme Research Laboratories. Urokinase was purchased from Abbott Laboratories. Tissue kallikrein-1 (HK-1) was purchased from Dr. Julie Chao, Medical University of South Carolina. Trypsin and chymotrypsin were purchased from Sigma Aldrich.

Recombinant factor VIIa was purchased from Novo Nordisk. Recombinant soluble tissue factor residues 1-219 was produced at Bristol-Myers Squibb.

Factor XIa, factor XIIa, chymotrypsin, tPA, plasmin and urokinase assays were conducted in 50 mM HEPES pH 7.4, 145 mM sodium chloride, 5 mM potassium chloride, and 0.1% PEG 8000. Factor Xa, thrombin, trypsin, plasma kallikrein, HK-1, and aPC assays were conducted in 100 mM sodium phosphate pH 7.4, 200 mM sodium chloride, and 0.5% PEG 8000. Factor VIIa assays were conducted in 50 mM HEPES pH 7.4, 150 mM sodium chloride, 5 mM calcium chloride, and 0.1% PEG 8000. Factor IXa assays were conducted in 50 mM TRIS pH 7.4, 100 mM sodium chloride, 5 mM calcium chloride, 0.5% PEG 8000 and 2% DMSO. The peptide substrates were: pyro-Glu-Pro-Arg-pNA(*para*-nitroaniline), (Diapharma) for factor XIa, thrombin, and aPC; N-benzoyl-Ile-Glu-(OH, OMe)-Gly-Arg-pNA (Diapharma) for factor Xa and trypsin; Methylsulfonyl-D-cyclohexylglycyl-Gly-Arg-AMC(7-amino-4-methylcoumarin) (Pentapharm) for factor IXa; H-(D)-Ile-Pro-Arg-pNA (Diapharma) for factor VIIa; H-(D)-CHT-Gly-Arg-pNA (American Diagnostica) for factor XIIa; H-(D)-Pro-Phe-Arg-pNA (Diapharma) for plasma kallikrein; MeO-Suc-Arg-Pro-Tyr-pNA (Diapharma) for chymotrypsin; H-(D)-Val-Leu-Lys-pNA (Diapharma) for plasmin; Methylsulfonyl-D-cyclohexylalanyl-Gly-Arg-pNA (American Diagnostica) for tPA; pyro-Glu-Gly-Arg-pNA (Diapharma) for urokinase; H-D-Val-Leu-Arg-AFC(7-amino-4-trifluoromethylcoumarin) (Calbiochem) for tissue kallikrein-1.

All assays were conducted at 37 °C, except where noted, in 96-well microtiter plate spectrophotometers or spectrofluorimeters (Molecular Devices) with simultaneous measurement of enzyme activities in control and inhibitor containing solutions. Compounds were dissolved and diluted in DMSO and analyzed at a final concentration of 1% DMSO except where noted. Assays were initiated by adding enzyme to buffered solutions containing substrate in the

presence or absence of inhibitor. Hydrolysis of the substrate resulted in the release of pNA (*para*-nitroaniline), which was monitored spectrophotometrically by measuring the increase in absorbance at 405 nm, or the release of AMC (7-amino-4-methylcoumarin), which was monitored spectrofluorometrically by measuring the increase in emission at 460 nm with excitation at 380 nm, or the release of AFC (7-amino-4-trifluoromethylcoumarin), which was monitored spectrofluorometrically by measuring the increase in emission at 505 nm with excitation at 400 nm. The rate of absorbance or fluorescence change is proportional to enzyme activity. A decrease in the rate of absorbance or fluorescence change in the presence of inhibitor is indicative of enzyme inhibition. Assays were conducted under conditions of excess substrate (up to 4 times K_m) and inhibitor over enzyme. The Michaelis constant, K_m, for substrate hydrolysis by each protease was determined by fitting data from independent measurements at several substrate concentrations to the Michaelis-Menten equation: $v = (V_{max}*[S])/(K_m + [S])$ where v is the observed velocity of the reaction; V_{max} is the maximal velocity; [S] is the concentration of substrate; K_m is the Michaelis constant for the substrate.

Values of IC_{50} were determined by allowing the protease to react with the substrate in the presence of the inhibitor. Reactions were allowed to go for periods of 10-120 minutes (depending on the protease) and the velocities (rate of absorbance or fluorescence change versus time) were measured. The following relationships were used to calculate IC_{50} values: $v_s/v_o = A + ((B-A)/(1 + (IC_{50}/I)^n))$ and where v_o is the velocity of the control in the absence of inhibitor; v_s is the velocity in the presence of inhibitor; I is the concentration of inhibitor; A is the minimum activity remaining (usually locked at zero); B is the maximum activity remaining (usually locked at 1.0); n is the Hill coefficient, a measure of the number and cooperativity of potential inhibitor binding sites; IC_{50} is the concentration of inhibitor that produces 50% inhibition. When

negligible enzyme inhibition was observed at the highest inhibitor concentration tested the value assigned as a lower limit for IC_{50} is the value that would be obtained with either 25% or 50% inhibition at the highest inhibitor concentration. In all other cases IC_{50} values represent the average of duplicate determinations obtained over 8 to 11 concentrations. The intraassay and interassay variabilities are 5% and 20%, respectively. Competitive inhibition was assumed for all proteases. IC_{50} values were converted to K_i values by the relationship: $K_i = IC_{50}/(1 + [S]/K_m)$.

Coagulation Assays. Coagulation assays were performed in a temperature-controlled automated coagulation device (Sysmex CA-6000 or CA-1500, Dade-Behring) according to the reagent manufacturer's instructions. Blood was obtained from healthy volunteers by venipuncture and anticoagulated with one-tenth volume 0.11 M buffered sodium citrate (Vacutainer, Becton Dickinson). Plasma was obtained after centrifugation at 2,000 g for 10 minutes and kept on ice prior to use. An initial stock solution of the inhibitor at 10 mM was prepared in DMSO. Subsequent dilutions were done in plasma. Clotting time was determined on control plasma, and plasma containing up to 7 different concentrations of inhibitor. Determinations were performed in duplicate and expressed as a mean ratio of treated vs. baseline control. The concentrations required to produce a 50% increase in the clotting time relative to the clotting time in the absence of the inhibitor ($EC_{1.5x}$) were calculated by linear interpolation (Microsoft Excel, Redmond, WA, USA) and are expressed as total plasma concentrations, not final assay concentrations after addition of clotting assay reagents. The aPTT reagents (Alexin or Actin® FSL) were from commercial sources. The aPTT reagent Actin® FSL, which was used after the aPTT reagent Alexin was discontinued by the vendor, was used for compounds **15**, **17**, **21**, and **23**.

ASSOCIATED CONTENT

Supporting Information

The supporting information is available free of charge on the ACS Publications website: http://pubs.acs.org. Analytical data and experimental procedures for both intermediate compounds **2a-2c**, **3b**, **3c**, **4c-4e**, **6b**, **7b-7d**, **8c-8h**, **9c-9g**, **11c-11f**, **12d-12f**, **14b**, **15a**, and final compounds **5-8**, **10**, **14**, **15**, **18-21**, and **23**; experimental procedure for pharmacokinetic studies; X-ray crystal structure of compound **13**; overlay of X-ray crystal structures of compounds **13** and **16**; crystallographic data and refinement statistics for X-ray structures of the FXIa complexes with compounds **9**, **13**, and **16**; assay for mechanism of FXIa inhibition; and conformational analysis of 11- to 14-membered rings.

Accession Codes

Crystallographic structures of **9**, **13**, and **16** complexed to Factor XIa have been deposited in the PDB as codes 5TKS, 5TKT, and 5TKU, repectively. Authors will release the atomic coordinates and experimental data upon article publication.

AUTHOR INFORMATION

Corresponding Author

*E-mail: james.corte@bms.com. Phone: 609-466-5030. Fax: 609-818-3331.

Notes

The authors declare no competing financial interest.

ACKNOWLEDGMENTS

The authors thank William R. Ewing and Ellen K. Kick for critical review of this manuscript; Atsu Apedo and Douglas B. Moore for chiral separations of intermediates; the Department of Discovery Synthesis, Madhavan Kannan, Rama Rao Abburi, and Karabasappa Mailar for the synthesis of intermediates at BMS Biocon Research Center; the Department of Lead Discovery & Optimization; Mojgan Abousleiman for in vitro work; Mei-Mann Hsueh, Gang Lou, Qinling Qu, and Baomin Xin for PK studies and analyses; Use of the IMCA-CAT beamline 17-ID at the Advanced Photon Source was supported by the companies of the Industrial Macromolecular Crystallography Association through a contract with Hauptman-Woodward Medical Research Institute. Use of the Advanced Photon Source was supported by the U. S. Department of Energy, Office of Science, Office of Basic Energy Sciences, under Contract No. DE-AC02-06CH11357.

ABBREVIATIONS USED

FXI, Factor XI; FXIa, Factor XIa; DVT, deep vein thrombosis; ACS, acute coronary syndrome; aPTT, activated partial thromboplastin time; $EC_{1.5x}$, effective concentration which produces a 50% increase in the clotting time relative to the clotting time in the absence of the inhibitor; HLM, human liver microsome; DLM, dog liver microsome; TPA, tissue plasminogen activator.

REFERENCES

1. GBD 2013 Mortality and Causes of Death Collaborators. Global, regional, and national age–sex specific all-cause and cause-specific mortality for 240 causes of death, 1990–2013: a systematic analysis for the global burden of disease study 2013. *Lancet* **2015**, *385*, 117-171.
2. (a) Morais, J.; De Caterina, R. Stroke prevention in atrial fibrillation: a clinical

perspective on trials of the novel oral anticoagulants. *Cardiovasc. Drugs Ther*. **2016**, *30*, 201-214. (b) Schaefer, J. K.; McBane, R. D.; Wysokinski, W. E. How to choose appropriate direct oral anticoagulant for patient with nonvalvular atrial fibrillation. *Ann. Hematol*. **2016**, *95*, 437–449. (c) Levy, J. H.; Spyropoulos, A. C.; Samama, C. M.; Douketis, J. Direct oral anticoagulants. *J. Am. Coll. Cardiol. Intv*. **2014**, *7*, 1333-1351.

3. (a) Cohen, A. T.; Spiro, T. E.; Buller, H. R.; Haskell, L.; Hu, D.; Hull, R.; Mebazaa, A.; Merli, G.; Schellong, S.; Spyropoulos, A. C.; Tapson, V.; MAGELLAN Investigators. Rivaroxaban for thromboprophylaxis in acutely ill medical patients. *N. Engl. J. Med*. **2013**, *368*, 513-523. (b) Goldhaber, S. Z.; Leizorovicz, A.; Kakkar, A. K.; Haas, S. K.; Merli, G.; Knabb, R. M.; Weitz, J. I.; ADOPT Trial Investigators. Apixaban versus enoxaparin for thromboprophylaxis in medically ill patients. *N. Engl. J. Med*. **2011**, *365*, 2167-2177.
4. (a) Mega, J. L.; Braunwald, E.; Wiviott, S. D.; Bassand, J-P.; Bhatt, D. L.; Bode, C.; Burton, P.; Cohen, M.; Cook-Bruns, N.; Fox, K. A. A.; Goto, S.; Murphy, S. A.; Plotnikov, A. N.; Schneider, D.; Sun, X.; Verheugt, F. W. A.; Gibson, C. M.; ATLAS ACS 2-TIMI 51 Investigators. Rivaroxaban in patients with a recent acute coronary syndrome. *N. Engl. J. Med*. **2012**, *366*, 9-19. (b) Alexander, J. H.; Lopes, R. D.; James, S.; Kilaru, R.; He, Y.; Mohan, P.; Bhatt, D. L.; Goodman, S.; Verheugt, F. W.; Flather, M.; Huber, K.; Liaw, D.; Husted, S. E.; APPRAISE-2 Investigators. Apixaban with antiplatelet therapy after acute coronary syndrome. *N. Engl. J. Med*. **2011**, *365*, 699-708.
5. In 2013 the European Union approved rivaroxaban for secondary prevention in ACS despite an increased risk of bleeding and intracranial hemorrhage. Please see (a) Behnes, M.; Fastner, C.; Ansari, U.; Akin, I. New oral anticoagulants in coronary artery

disease. *Cardiovasc. Hematol. Disord.: Drug Targets* **2015**, *15*, 101-105. (b) Oldgren, J.; Wallentin, L.; Alexander, J. H.; James, S.; Jonelid, B.; Steg, G.; Sundstrom, J. New oral anticoagulants in addition to single or dual antiplatelet therapy after an acute coronary syndrome: a systematic review and meta-analysis. *Eur. Heart J.* **2013**, *34*, 1670-1680.

6. (a) Emsley, J.; McEwan, P. A.; Gailani, D. Structure and function of factor XI. *Blood* **2010**, *115* (13), 2569-2577. (b) Gailani, D.; Renne, T. Intrinsic pathway of coagulation and arterial thrombosis. *Arterioscler. Thromb. Vasc. Biol*. **2007**, *27* (12), 2507-2513. (c) von dem Borne, P. A.; Meijers, J. C. M.; Bouma, B. N. Feedback activation of factor XI by thrombin in plasma results in additional formation of thrombin that protects fibrin clots from fibrinolysis. *Blood* **1995**, *86* (8), 3035-3042.
7. Bane, C. E.; Neff, A. T.; Gailani, D. Factor XI deficiency or hemophilia C. In *Hemostasis and Thrombosis: Practical Guidelines in Clinical Management*; Saba, H.I., Roberts, H. R., Eds.; John Wiley & Sons, Ltd.: Oxford, 2014; pp 71-81.
8. (a) Salomon, O.; Steinberg, D. M.; Koren-Morag, N.; Tanne, D.; Seligsohn, U. Reduced incidence of ischemic stroke in patients with severe factor XI deficiency. *Blood* **2008**, *111* (8), 4113-4117. (b) Salomon, O.; Steinberg, D. M.; Dardik, R.; Rosenberg, N.; Zivelin, A.; Tamarin, I.; Ravid, B.; Berliner, S.; Seligsohn, U. Inherited factor XI deficiency confers no protection against acute myocardial infarction. *J. Thromb. Haemost.* **2003**, *1*, 658-661. (c) Salomon, O.; Steinberg, D. M.; Zucker, M.; Varon, D.; Zivelin, A.; Seligsohn, U. Patients with severe factor XI deficiency have a reduced incidence of deep-vein thrombosis. *Thromb. Haemost*. **2011**, *105*, 269-273.
9. (a) Doggen, C. J. M; Rosendaal, F. R.; Meijers, J. C. M. Levels of intrinsic coagulation factors and the risk of myocardial infarction among men: opposite and synergistic effects

of factor XI and XII. *Blood* **2006**, *108* (13), 4045-4051. (b) Meijers, J. C. M.; Tekelenburg, W. L. H.; Bouma, B. N.; Bertina, R. M.; Rosendaal, F. R. High levels of coagulation factor XI as a risk factor for venous thrombosis. *N. Eng. J. Med.* **2000**, *342*(10), 696-701.

10. (a) Bane, C. E.; Gailani, D. Factor XI as a target for antithrombotic therapy. *Drug Discovery Today* **2014**, *19* (9), 1454-1458. (b) Muller, F.; Gailani, D.; Renne, T. Factor XI and XII as antithrombotic targets. *Curr. Opin. Hematol.* **2011**, *18*, 349-355.
11. (a)Yamashita, A.; Nishihira, K.; Kitazawa, T.; Yoshihashi, K.; Soeda, T.; Esaki, K.; Imamura, T.; Hattori, K.; Asada, Y. Factor XI contributes to thrombus propagation on injured neotima of the rabbit iliac artery. *J. Thromb. Haemost.* **2006**, *4*, 1496-1501. (b) Tucker, E. I.; Marzec, U. M.; White, T. C.; Hurst, S.; Rugonyi, S.; McCarty, O. J. T.; Gailani, D.; Gruber, A.; Hanson, S. R. Prevention of vascular graft occlusion and thrombus-associated thrombin generation by inhibition of factor XI. *Blood* **2009**, *113* (4), 936-944. (c) Gruber, A.; Hanson, S. R. Factor XI-dependence of surface- and tissue-initiated thrombus propagation in primates. *Blood* **2003**, *102* (3), 953-955.
12. (a) Crosby, J. R.; Marzec, U.; Revenko, A. S.; Zhao, C.; Gao, D.; Matafonov, A.; Gailani, D.; MacLeod, A. R.; Tucker, E. I.; Gruber, A.; Hanson, S.; Monia, B. P. Antithrombotic effect of antisense factor XI oligonucleotide treatment in primates. *Arterioscler. Thromb. Vasc. Biol.* **2013**, *33*, 1670-1678. (b) Zhang, H.; Lowenberg, E. C.; Crosby, J. R.; MacLeod, A. R.; Zhao, C.; Gao, D.; Black, C.; Revenko, A. S.; Meijers, J. C. M., Stroes, E. S.; Levi, M.; Monia, B. P. Inhibition of the intrinsic coagulation pathway factor XI by antisense oligonucleotides: a novel antithrombotic strategy with lowered bleeding risk. *Blood* **2010**, *116*, 4684-4692.

13. Buller, H. R.; Bethune, C.; Bhanot, S.; Gailani, D.; Monia, B. P.; Raskob, G. E.; Segers, A.; Verhamme, P.; Weitz, J. I. Factor XI antisense oligonucleotide for prevention of venous thrombosis. *N. Engl. J. Med*. **2015**, *372*, 232-240. The FXIa ASO work published subsequent to the work described herein.

14. (a) Schumacher, W. A.; Seiler, S. E.; Steinbacher, T. E.; Stewart, A. B.; Bostwick, J. S.; Hartl, K. S.; Liu, E. C.; Ogletree, M.L. Antithrombotic and hemostatic effects of small molecule factor XIa inhibitor in rats. *Eur. J. Pharmacol.* **2007**, *570*, 167-174. (b) Wong, P. C.; Crain, E. J.; Watson, C. A.; Schumacher, W. A. A small-molecule factor XIa inhibitor produces antithrombotic efficacy with minimal bleeding time prolongation in rabbits. *J. Thromb. Thrombolysis* **2011**, *32*, 129-137.

15. (a) Deng, H.; Bannister, T. D.; Jin, L.; Babine, R. E.; Quinn, J.; Nagafuji, P.; Celatka, C. A.; Lin, J.; Lazarova, T. I.; Rynkiewicz, M. J.; Bibbins, F.; Pandey, P.; Gorga, J.; Meyers, H. V.; Abdel-Meguid, S. S.; Strickler, J. E. Synthesis, SAR exploration, and x-ray crystal structures of factor XIa inhibitors containing an α-ketothiazole arginine. *Bioorg. Med. Chem. Lett.* **2006**, *16*, 3049-3054. (b) Lin, J.; Deng, H.; Jin, L.; Pandey, P.; Quinn, J.; Cantin, S.; Rynkiewicz, M. J.; Gorga, J. C.; Bibbins, F.; Celatka, C. A.; Nagafuji, P.; Bannister, T. D.; Meyers, H. V.; Babine, R. E.; Hayward, N. J.; Weaver, D.; Benjamin, H.; Stassen, F.; Abdel-Meguid, S. S.; Strickler, J. E. Design, synthesis, and biological evaluation of peptidomimetic inhibitors of factor XIa as novel anticoagulants. *J. Med. Chem.* **2006**, *49*, 7781-7791.

16. Boronic acid peptidomimetics and the natural product clavatadine A are also examples of active site irreversible FXIa inhibitors but they have not been studied in preclinical thrombosis models, please see (a) Lazarova, T. I.; Jin, L.; Rynkiewicz, M.; Gorga, J.C.;

Bibbins, F.; Meyers, H. V.; Babine, R.; Strickler, J. Synthesis and in vitro biological evaluation of aryl boronic acids as potential inhibitors of factor XIa. *Bioorg. Med. Chem. Lett.* **2006**, *16*, 5022-5027. (b) Buchanan, M. S.; Carroll, A. R.; Wessling, D.; Jobling, M.; Avery, V. M.; Davis, R. A.; Feng, Y.; Xue, Y.; Oster, L.; Fex, T.; Deinum, J.; Hooper, J. N. A.; Quinn, R. J. Clavatadine A, a natural product with selective recognition and irreversible inhibition of factor XIa. *J. Med. Chem.* **2008**, *51*, 3583-3587.

17. Al-Horani, R. A.; Desai, U. R. Designing allosteric inhibitors of factor XIa. Lessons from the interactions of sulfated pentagalloylglucopyranosides. *J. Med. Chem*. **2014**, *57*(11), 4805-4818. (b) Sinha, D.; Badellino, K. O.; Marcinkiewicz, M.; Walsh, P. N. Allosteric modification of factor XIa functional activity upon binding to polyanions. *Biochemistry* **2004**, *43*, 7593-7600.
18. (a) Quan, M .L.; Wong, P. C.; Wang, C.; Woerner, F.; Smallheer, J. M.; Barbera, F. A.; Bozarth, J. M.; Brown, R. L.; Harpel, M. R.; Luettgen, J. M.; Morin, P. E.; Peterson, T.; Ramamurthy, V.; Rendina, A. R.; Rossi, K. A.; Watson, C. A.; Wei, A.; Zhang, G.; Seiffert, D.; Wexler, R. R. Tetrahydroquinoline derivatives as potent and selective factor XIa inhibitors. *J. Med. Chem*. **2014**, *57*(3), 955-969. (b) Wong, P. C.; Quan, M. L.; Watson, C. A.; Crain, E. J.; Harpel, M. R.; Rendina, A. R.; Luettgen, J. M.; Wexler, R. R.; Schumacher, W. A.; Seiffert, D. A. In vitro, antithrombotic and bleeding time studies of BMS-654457, a small-molecule, reversible and direct inhibitor of factor XIa. *J. Thromb. Thrombolysis* **2015**, *40*(4), 416-423.
19. Smallheer, J. M.; Wang, S.; Rossi, K. A.; Rendina, A.; Morin, P. E.; Wei, A.; Zhang, G.; Wong, P. C.; Seiffert, D.; Wexler, R. R.; Quan, M. L. Biarylmethyl indoline and indole analogs as potent and selective inhibitors of factor XIa. Presented at the 245th National

Meeting of the American Chemical Society, New Orleans, LA, April 2013; MEDI-415.

20. Hangeland, J. J.; Friends, T. J.; Rossi, K. A.; Smallheer, J. M.; Wang, C.; Sun, Z.; Corte, J. R.; Fang, T.; Wong, P. C.; Rendina, A. R.; Barbera, F. A.; Bozarth, J. M.; Luettgen, J. M.; Watson, C. A.; Zhang, G.; Wei, A.; Ramamurthy, V.; Morin, P. E.; Bisacchi, G. S.; Subramaniam, S.; Arunachalam, P.; Mathur, A.; Seiffert, D. A.; Wexler, R. R.; Quan, M. L. Phenylimidazoles as potent and selective inhibitors of coagulation factor XIa with in vivo antithrombotic activity. *J. Med. Chem*. **2014**, *57*, 9915-9932.
21. (a) Pinto, D. J. P; Smallheer, J. M.; Corte, J. R.; Austin, E. J. D.; Wang, C.; Fang, T., Smith, L. M.; Rossi, K. A.; Rendina, A. R.; Bozarth, J. M.; Zhang, G.; Wei, A.; Ramamurthy, V.; Sheriff, S.; Myers, J. E.; Morin, P. E.; Luettgen, J. M.; Seiffert, D. A.; Quan, M. L.; Wexler, R. R. Structure-based design of inhibitors of coagulation factor XIa with novel P1 moieties. *Bioorg. Med. Chem. Lett.* **2015**, *25*, 1635-1642. (b) Hu, Z.; Wong, P. C.; Gilligan, P. J.; Han, W.; Pabbisetty, K. B.; Bozarth, J. M.; Crain, E. J.; Harper, T.; Luettgen, J. M.; Myers, J. E.; Ramamurthy, V.; Rossi, K. A.; Sheriff, S.; Watson, C. A.; Wei, A.; Zheng, J. J.; Seiffert, D. A.; Wexler, R. R.; Quan, M. L. Discovery of a potent parenterally administered factor XIa inhibitor with hydroxyquinolin-2(1H)-one as the P2' moiety. *ACS Med. Chem. Lett.* **2015**, *6*, 590-595.
22. (a) Corte, J. R; Fang, T.; Hangeland, J. J.; Friends, T. J.; Rendina, A. R.; Luettgen, J. M.; Bozarth, J. M.; Barbera, F. A.; Rossi, K. A.; Wei, A.; Ramamurthy, V.; Morin, P. E.; Seiffert, D. A.; Wexler, R. R.; Quan, M. L. Pyridine and pyridinone-based factor XIa inhibitors. *Bioorg. Med. Chem. Lett.* **2015**, *25*, 925-930. (b) Corte, J. R.; Fang, T.; Pinto, D. J. P.; Orwat, M. J.; Rendina, A. R.; Luettgen, J. M.; Rossi, K. A.; Wei, A.; Ramamurthy, V.; Myers, J. E.; Sheriff, S.; Narayanan, R.; Harper, T. W.; Zheng, J. J.; Li,

Y.; Seiffert, D. A.; Wexler, R. R.; Quan, M. L. Orally bioavailable pyridine and pyrimidine-based factor XIa inhibitors: discovery of the methyl N-phenyl carbamate P2 prime group. *Bioorg. Med. Chem.* **2016**, *24*, 2257-2272.

23. Smith, L. M.; Orwat, M. J.; Hu, Z.; Han, W.; Wang, C.; Rossi, K. A.; Gilligan, P. J.; Pabbisetty, K. B.; Osuna, H.; Corte, J. R.; Rendina, A. R.; Luettgen, J. M.; Wong, P. C.; Narayanan, R.; Harper, T. W.; Bozarth, J. M.; Crain, E. J.; Wei, A.; Ramamurthy, V.; Morin, P. E.; Xin, B.; Zheng, J.; Seiffert, D. A.; Quan, M. L.; Lam, P. Y. S.; Wexler, R. R.; Pinto, D. J. P. Novel phenylalanine derived diamides as factor XIa inhibitors. *Bioorg. Med. Chem. Lett.* **2016**, *26*, 472-478.
24. An active site reversible FXIa inhibitor based on a diamide chemotype was also recently disclosed, please see: Fjellstrom, O.; Akkaya, S.; Beisel, H. G.; Eriksson, P. O.; Erixon, K.; Gustafsson, D.; Jurva, U.; Kang, D.; Karis, D.; Knecht, W.; Nerme, V.; Nilsson, I.; Olsson, T.; Redzic, A.; Roth, R.; Sandmark, J.; Tigerstrom, A.; Oster, L. Creating novel activated factor XI inhibitors through fragment based lead generation and structure aided drug design. *PLoS One* **2015,** *10*, e0113705.
25. (a) Driggers, E. M.; Hale, S. P.; Lee, J.; Terrett, N. K. The exploration of macrocycles for drug discovery-an underexploited structural class. *Nat. Rev. Drug Discov*. **2008**, *7*(7), 608-624. (b) Marsault, E.; Peterson, M. L. Macrocycles are great cycles: applications, opportunities, and challenges of synthetic macrocycles in drug discovery. *J. Med. Chem*. **2011**, *54*, 1961-2004. (c) Mallinson, J.; Collins, I. Macrocycles in new drug discovery. *Future Med. Chem*. **2012**, *4*, 1409-1438.
26. Giordanetto, F.; Kihlberg, J. Macrocyclic drugs and clinical candidates: what can medicinal chemists learn from their properties? *J. Med. Chem*. **2014**, *57*, 278-295.

27. (a) Nantermet, P. G.; Barrow, J. C.; Newton, C. L.; Pellicore, J. M.; Young, M.; Lewis, S. D.; Lucas, B. J.; Krueger, J. A.; McMasters, D. R.; Yan, Y.; Kuo, L. C.; Vacca, J. P.; Selnick, H. G. Design and synthesis of potent and selective macrocyclic thrombin inhibitors. *Bioorg. Med. Chem. Lett.* **2003**, *13*, 2781-2784. (b) For studies on the macrocyclic natural product cyclotheonamide A, please see: Greco, M. N.; Powell, E. T.; Hecker, L. R.; Andrade-Gordon, P.; Kauffman, J. A.; Lewis, J. M.; Ganesh, V.; Tulinsky, A.; Maryanoff, B. E. Novel thrombin inhibitors that are based on a macrocyclic tripeptide motif. *Bioorg. Med. Chem.* **1996**, *6*, 2947-2952.

28. Priestley, E. S.; Cheney, D. L.; DeLucca, I.; Wei, A.; Luettgen, J. M.; Rendina, A. R.; Wong, P. C.; Wexler, R. R. Structure-based design of macrocyclic coagulation factor VIIa inhibitors. *J. Med. Chem*. **2015**, *58*, 6225-6236.

29. Van Lierop, B. J.; Lummiss, J. A. M.; Fogg, D. E. Ring-closing metathesis. In *Olefin Metathesis: Theory and Practice*; Grela, K., Ed.; John Wiley & Sons Inc.: Hoboken, New Jersey, 2014; pp 85-152.

30. Contour-Galcera, M.; Poitout, L.; Moinet, C.; Morgan, B.; Gordon, T.; Roubert, P.; Thurieau, C. Synthesis of substituted imidazopyrazines as ligands for the human somatostatin receptor subtype 5. *Bioorg. Med. Chem. Lett.* **2001**, *11*, 741-745.

31. Zou, G.; Reddy, Y. K.; Falck, J. R. Ag(I)-promoted Suzuki-Miyaura cross-coupling of n-alkylboronic acids. *Tetrahedron Lett*. **2001**, *42*, 7213-7215.

32. Kim, J.; Chang, S. Ammonium salts as an inexpensive and convenient nitrogen source in the Cu-catalyzed amination of aryl halides at room temperature. *Chem. Commun*. **2008**, 3052-3054.

33. Cai, Q.; Zhu, W.; Zhang, H.; Zhang, Y.; Ma, D. Preparation of N-aryl compounds by

amino acid-promoted Ullmann-type coupling reactions. *Synthesis*, **2005**, *37*, 496-499. It was interesting to note that the azide was reduced to the aniline in situ which had not been observed in this reference.

34. Chen, Y.; Dias, H. V. R.; Lovely, C. J. Synthesis of fused bicyclic imidazoles by ring-closing metathesis. *Tetrahedron Lett*. **2003**, *44*, 1379-1382.
35. The Z-alkene analogs in both the 12- and 13-membered alkyl-linked macrocycles showed a significant loss in FXIa activity, unpublished results from Corte, J.
36. The increase in dihedral angle was a common feature for the macrocyclic series. The X-ray crystal structure of the 12-membered macrocycle **3** revealed a 23^{o} increase in the dihedral angle of the P2 prime phenyl compared to acyclic phenyl imidazole **1**, unpublished results from Sheriff, S. and Rossi, K. A.
37. The NH of the carbamate forms a hydrogen bond with the carbonyl of His40 (2.9 Å) and the carbonyl of the carbamate forms a hydrogen bond through a conserved water to Ile151 (2.7 Å).
38. For numbering, the benzylic carbon of the macrocyclic linker is designated C1. The distances from the linker in macrocycle **9** to the disulfide bridge are: C3 to CYS42 (5.6Å) and CYS58 (6.5Å); C4 to CYS42 (4.4Å) and CYS58 (5.1Å); and C5 to CYS42 (4.2Å) and CYS58 (4.7Å).
39. The significant loss in FXIa affinity, on going from the amide/carbamate-linked macrocycles to the amine-linked macrocycle, may not be entirely due to the difference in H-bond donor ability of these different groups. We speculate that the amide/carbamate moieties also serve to reduce the conformational entropy of the macrocycle ring by rigidifying the macrocyclic linker.

40. The distances from the linker in macrocycle **16** to the disulfide bridge are: αC to CYS42 (4.4Å) and CYS58 (5.6Å); βC to CYS42 (4.8Å) and CYS58 (5.5Å); and γC to CYS42 (4.7Å) and CYS58 (5.3Å). The distances from the linker in macrocycle **13** to the disulfide bridge are: αC to CYS42 (4.6Å) and CYS58 (5.6Å); βC to CYS42 (4.8Å) and CYS58 (5.5Å); and γC to CYS42 (4.4Å) and CYS58 (5.0Å).

41. Pinto, D. J. P.; Orwat, M. J.; Koch, S.; Rossi, K. A.; Alexander, R. S.; Smallwood, A.; Wong, P. C.; Rendina, A. R.; Luettgen, J. M.; Knabb, R. M.; He, K.; Xin, B.; Wexler, R. R.; Lam, P. Y. S. Discovery of 1-(4-Methoxyphenyl)-7-oxo-6-[4-(2-oxo-1-piperidinyl] phenyl)-4,5,6,7-tetrahydro-1H-pyrazolo[3,4-c]pyridine-3-carboxamide (apixaban, BMS-562247), a highly potent, selective, efficacious, and orally bioavailable inhibitor of blood coagulation factor Xa. *J. Med. Chem.* **2007**, *50*(22), 5339-5356.

42. The amino acid sequence of plasma kallikrein has 58% homology to FXI, please see Renne, T.; Gailani, D.; Meijers, J. C. M.; Werner, M-E. Characterization of the H-kininogen-binding site on factor XI: a comparison of factor XI and plasma prekallikrein. *J. Biol. Chem*. **2002**, *277*, 4892-4899.

43. Otwinowski, Z.; Minor, W. Macromolecular Crystallography. Part A; Carter, C.W., Sweet, R.M., Eds.; *Methods in Enzymol.* Vol. 276; Academic Press, Inc.: San Diego, CA, 1997; pp 307-326.

44. Navaza, J. AMoRe: an automated package for molecular replacement. *Acta Crystallogr. Sect*. A **1994**, *50*, 157-163.

45. Navaza, J.; Vernoslova, E. On the fast translation functions for molecular replacement. *Acta Crystallogr. Sect. A* **1995**, *51*, 445-449.

46. Collaboration Computational Project, Number 4. The CCP4 suite: programs for protein

crystallography. *Acta Crystallogr Sect. D* **1994**, *50*, 760-763.

47. Blanc, E.; Roversi, P.; Vonrhein, C.; Flensburg, C.; Lea, S. M.; Bricogne, G. Refinement of severely incomplete structures with maximum likelihood in BUSTER/TNT. *Acta Crystallogr., Sect. D: Biol. Crystallogr.* **2004**, *60*, 2210-2221.
48. Emsley, P.; Lokhamp, B.; Scott, W.G.; Cowtan, K. Features and development of Coot. *Acta Crystallogr., Sect. D: Biol. Crystallogr.* **2010**, *66*, 486-501.

Table of Contents Graphic